# Chlorophylls as Primary Electron Acceptors in Reaction Centers: A Blueprint for Highly Efficient Charge Separation in Bio-inspired Artificial Photosynthetic Systems

Michael Gorka,<sup>a</sup> Patrick Landry,<sup>b</sup> Elijah Gruszecki,<sup>b</sup> Amanda Malnati,<sup>b</sup> Divya Kaur,<sup>c</sup> Art van der Est,<sup>c,d</sup> John H. Golbeck<sup>a,e,\*</sup> and K. V. Lakshmi<sup>b,\*</sup>

<sup>a</sup>Department of Chemistry, The Pennsylvania State University, University Park, PA 16802, USA
 <sup>b</sup>Department of Chemistry and Chemical Biology and The Baruch '60 Center for Biochemical Solar Energy Research, Rensselaer Polytechnic Institute, Troy, NY 12180, USA
 <sup>c</sup>Department of Chemistry and <sup>d</sup>Department of Physics, Brock University, 1812 Sir Isaac Brock Way, St. Catharines, ON L2S 3A1, Canada
 <sup>e</sup>Department of Biochemistry and Molecular Biology, The Pennsylvania State University, University Park, PA 16802, USA

#### **Correspondence:**

K. V. Lakshmi Department of Chemistry and Chemical Biology Rensselaer Polytechnic Institute Troy, NY 12180, USA

E-mail: <u>lakshk@rpi.edu</u> Phone: (518) 698 7976

John H. Golbeck
Departments of Biochemistry and Molecular Biology and Chemistry
The Pennsylvania State University
State College, PA 16802, USA
E-mail: jhg5@psu.edu

Phone: (814) 865 1163

Keywords: Primary acceptor, charge separation, Reaction Center, Type I, Type II, heterodimer, homodimer, chlorophyll, electron paramagnetic resonance (EPR) spectroscopy, density functional theory (DFT).

#### Abstract.

Photosynthetic Reaction Centers (RCs) can be considered blueprints for highly efficient energy transfer. Embedded with an array of cofactors, including (bacterio)chlorophyll ((B)Chl) and (B)pheophytin ((B)Pheo) molecules, RCs function with a high quantum yield that spans a wide spectral range. Understanding the principles that underlie their function can influence the design of the next generation of artificial photosynthetic devices. We are particularly interested in the factors that influence the early stages of light-driven charge separation in RCs. With the recent publication of several highly anticipated RC structures and advanced computational methods available, it is possible to probe both the geometric and electronic structures of an array of RCs. In this chapter, we review the electronic and geometric structures of the (B)Chl and (B)Pheo primary electron acceptors from five RCs, comprising both Type I and Type II RCs and representing both heterodimeric and homodimeric systems. We showcase the dimeric  $A_0^{\bullet}$  state of Type I RCs, whereby the unpaired electron is delocalized, to various extents, over two (B)Chl molecules, (B)Chl<sub>2</sub> and (B)Chl<sub>3</sub>. This delocalization is controlled by several factors, including the structure of the (B)Chls, interactions with the surrounding protein matrix, and the orientation and distances of the cofactors themselves. In contrast, the primary acceptors of Type II RCs are entirely monomeric, with electron density residing solely on the (B)Pheo. We compare the natural design of the primary acceptors of the Type I and Type II RCs from both an evolutionary and application based perspective.

#### Introduction.

Photosynthesis has powered the planet for the past 3.4 billion years through its ability to convert light energy into chemical energy. It is one of the most important processes in nature as these reactions ultimately drive CO<sub>2</sub> fixation, which provides the energy rich compounds needed to support nearly all life on earth. The early stages of photosynthesis occur in three steps, namely, light capture, photoexcitation, and the generation of reducing equivalents through electron transfer; each occurring with unrivaled efficiency. The quantum efficiency of light capture, aided by photosensitive pigments, reaches 0.97 and the efficiency of photoexcitation and electron throughput approaches unity, across a wide region of wavelengths in the visible and near IR region of the electromagnetic spectrum.

The primary photosensitive pigment used in photosynthesis is chlorophyll (Chl), which consists of a tetrapyrrole macrocycle with an extended  $\pi$ -system that binds a central Mg<sup>2+</sup> or Zn<sup>2+</sup> ion. 9-11 Chlorophyll molecules serve multiple functions in photosynthesis, ranging from light harvesting to electron transfer. The versatility of these pigments to perform a wide variety of functions stems largely from their stability within a protein matrix, long excited singlet state lifetimes, and the tunability of their optical and redox properties. 12, 13 Apart from the Chls found in oxygenic photosynthetic organism, there are two other subsets of Chls: bacteriochlorophylls (BChl) and divinylchlorophylls (DVChl), which are also prevalent in photosynthesis. BChls are most often found in anoxygenic phototrophs and are differentiated by the extent of  $\pi$ -bond delocalization over the macrocycle, 14 while DVChls are found in organisms that survive on blue light, which is available deeper in the water column. 15-19 It is interesting that the modification of an ethyl group of a pyrrole ring on a Chl to a vinyl group in DVChls alters the characteristic wavelength of absorbance without altering other important functional properties. 15 Both Chls and BChls occur in a variety of 'flavors' or types, as designated by the specific letter after the pigment identity (e.g. (B)Chl a, (B)Chl b and (B)Chl g), which arise from changes and substitutions within the tetrapyrrole macrocycle. Even small changes that impact the extended  $\pi$ system result in non-trivial changes of the absorbance characteristics, which allows certain organisms to better survive where different wavelengths of light are more plentiful. 15, 18, 20, 21 Another important (B)Chl derivative in photosynthesis is (bacterio)pheophytin, (B)Pheo, which lacks a central metal ion. For a detailed description of Chl molecules and their derivatives, please refer to (12, 22). 12, 22

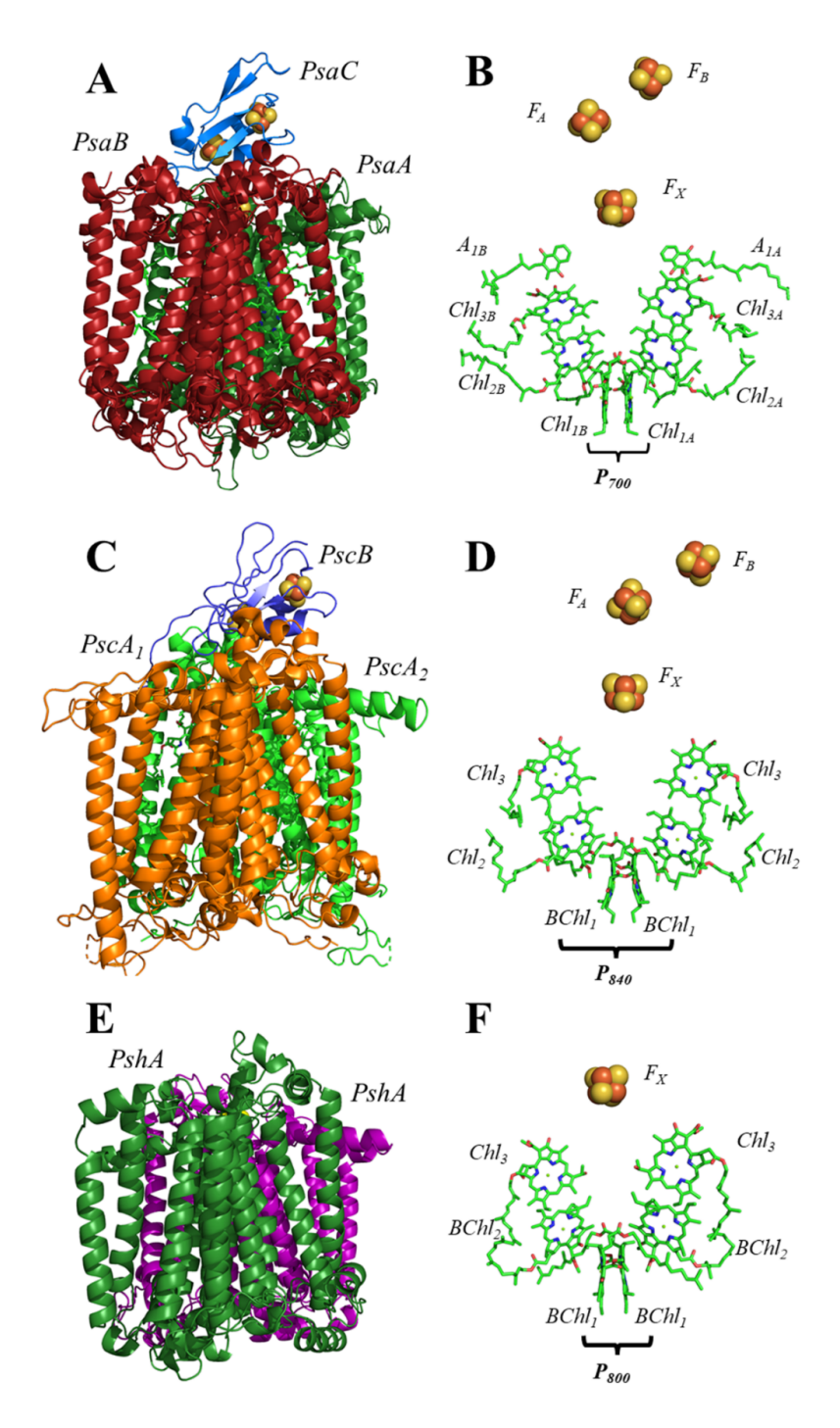


**Figure 1**. The structure of the three Type I RCs discussed in this study. The **(A)** three core subunits of PSI (PDB: 1jb0); PsaA (green), PsaB (red), and PsaC (green) and **(B)** electron transfer cofactors embedded within PSI.<sup>2</sup> The **(C)** three core subunits of the GsbRC (PDB: 6m32); PscA/B (orange/green), and PscB (blue) and **(D)** electron transfer cofactors embedded within the GsbRC.<sup>4</sup> The **(E)** core subunits of the homodimeric HbRC (PDB: 5v8k) and **(F)** bound electron transfer cofactors embedded within the HbRC.<sup>5</sup>

The (B)Chl and (B)Pheo molecules involved in photosynthesis and are bound to a wide

variety of light-harvesting proteins and in the reaction centers (RCs). The RCs are multi-subunit membrane protein complexes found in the photosynthetic membranes of the cell. Together with the light harvesting proteins, RCs harvest light energy via absorption and subsequent energy and electron transfer reactions, which result in the storage of reducing equivalents and creation of the proton gradient needed for the synthesis of ATP. In photoautotrophic organisms, these energy rich compounds are then used in CO<sub>2</sub> fixation reactions. In addition to (B)Chls that are used for both light harvesting and electron transfer, RCs also contain inorganic cofactors, such as a nonheme iron atom, four iron-four sulfur [4Fe-4S] clusters,<sup>2</sup> and the unique tetranuclear manganesecalcium-oxo (Mn<sub>4</sub>Ca-oxo) cluster that acts as a water-splitting catalyst.<sup>3</sup> The overall structure of the various RCs is highly conserved across all photosynthetic organisms and is comprised of two major polypeptides at its core, with several smaller intrinsic or extrinsic subunits that are either tightly or loosely bound to the complex. Most of the redox-active cofactors that participate in electron transfer from the lumenal to the stromal side of the membrane are bound to the core polypeptide subunits, while light harvesting pigments that facilitate energy transfer are arranged around the redox cofactors and are bound to a variety of polypeptide subunits or separate light harvesting protein complexes.<sup>2, 3</sup>

The electron transfer cofactors in all known RCs share a common structure motif of two branches and cofactors extending across the membrane in a roughly  $C_2$  symmetric arrangement. However, there are differences in the number and types of cofactors. There are two major classes of RCs, Type I and Type II, with several distinctive features. The most pronounced difference between the two types of RCs is the identity of the terminal electron acceptors. In Type I RCs, the terminal electron acceptor is always a [4Fe–4S] cluster that undergoes single electron reduction (Figure 1A-F).<sup>2, 4, 5</sup> In contrast, the terminal acceptor in Type II RCs is a labile quinone (Figure 2A-D), which is a two-electron two-proton acceptor.<sup>1, 3</sup> Moreover, Type I and Type II RCs also differ in the nature, identity, and orientation of the primary electron acceptor. Both types of RCs contain a combination of six (B)Chl and/or (B)Pheo molecules that are responsible for the initial charge separation reaction. Common to both types of RCs is a pair of strongly excitonically coupled (B)Chl molecules (Chl<sub>1A/1B</sub>), that are closely spaced and adopt a near parallel ring orientation (see 22 for a review). This dimer, or "special pair", acts as an electron donor and is assigned the spectroscopic label,  $P_{\lambda}$ , where  $\lambda$  is the maximum wavelength of absorption of the cofactor. Here we will refer to the dimer as the primary donor although the

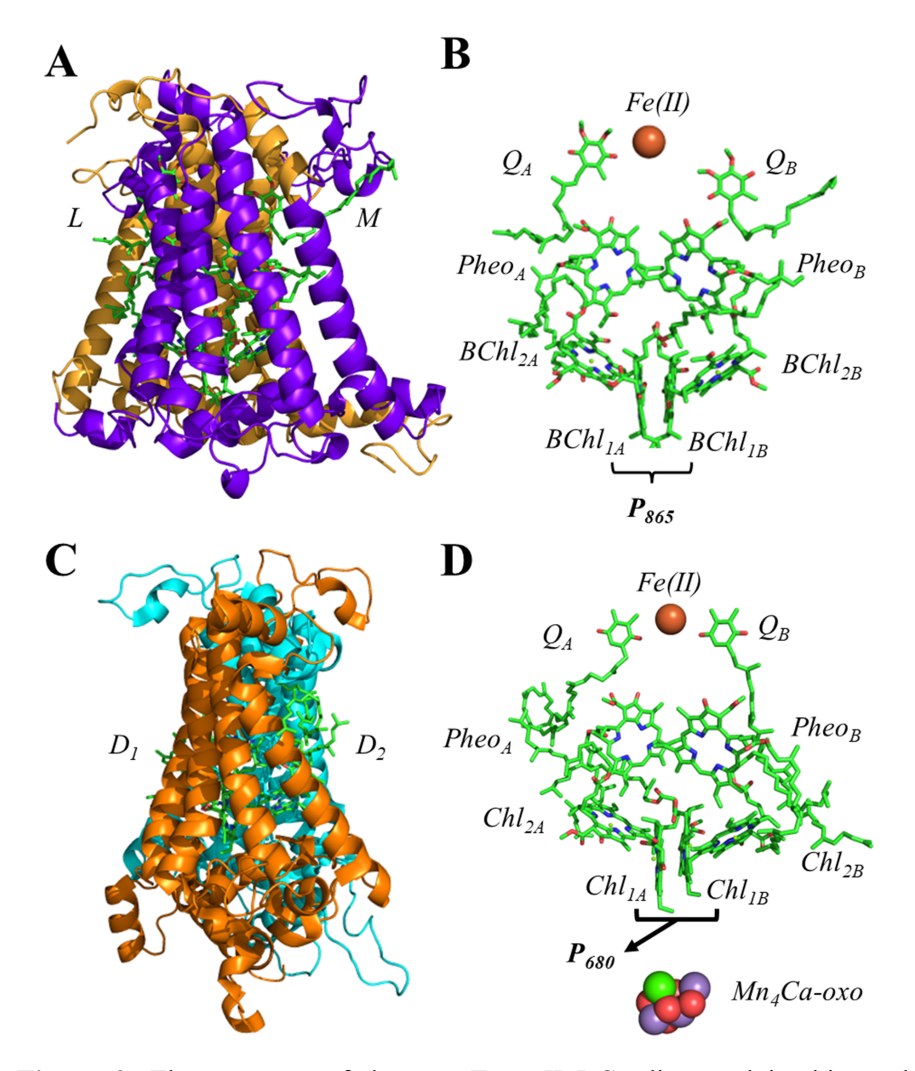


**Figure 2.** The structure of the two Type II RCs discussed in this study. The **(A)** bRC from *Rba.* sphaeroides I (PDB: 1aij)<sup>I</sup>, and **(B)** its electron transfer cofactors and **(C)** PSII from the thermophilic bacterium T. vulcanus (PDB: 3wu2)<sup>I</sup> and **(D)** its electron transfer cofactors.

site of the initial charge separation is still under debate in some RCs. On either side of the primary donor are two so called accessory Chls (Chl<sub>2A/2B</sub>) that often (but not exclusively) of the same type as the (B)Chls in the primary donor. The next cofactor in each branch (Chl<sub>3A/3B</sub>) acts as an electron acceptor and differs between the two types of RCs. In Type I RCs, Chl<sub>3A/3B</sub> is a (B)Chl molecule (**Figure 1A-F**), while Type II RCs contain a (B)Pheo, which is of the same type as the (B)Chl molecules in the primary donor (**Figure 2A-D**). There is a significant difference in the relative orientation of (B)Chl<sub>2</sub>/(B)Pheo in Type II RCs in comparison with (B)Chl<sub>2</sub>/(B)Chl<sub>3</sub> in Type I RCs. For example, in Type I RCs, the (B)Chl<sub>2</sub>/(B)Chl<sub>3</sub> pair always adopts a parallel orientation with significant overlap of the (B)Chl

rings, which is very similar to the primary donor. However, the orientation of the (B)Chl<sub>2</sub>/(B)Pheo pair in Type II RCs is nearly orthogonal with negligible overlap of the (B)Chl<sub>2</sub> and (B)Pheo rings.

The Type I RCs are further categorized as homodimers and heterodimers, based on the nature of the core polypeptide subunits. Homodimeric RCs are formed when a single copy of a gene is responsible for coding the two major subunits in the RC core, e.g. the RC from Chlorobaculum tepidum, where the PscA subunits are coded by the pscA gene. 23, 24 In contrast, heterodimeric RCs have two distinct polypeptide subunits that house the electron-transfer cofactors. Most often this originates from two separate genes that each code for one of the two polypeptide core subunit, with a notable exception being the Type II RC from Roseiflexus castenholzii whose heterodimeric core is coded by the DSM 13941 gene.<sup>25, 26</sup> While homodimeric RCs are completely symmetric (Figure 1C-F) with exact c<sub>2</sub> symmetry, heterodimeric RCs display only pseudo-c<sub>2</sub> symmetry (Figure 1A-B), resulting in different electron transfer energetics and rates in the two branches. All known Type II RCs and PSI<sup>1, 3, 27-31</sup> are heterodimeric in nature (Figure 2A-D), and the other Type I RCs are homodimeric.<sup>4, 5</sup> In PSI, this manifests as a preference for A-branch electron transfer by a factor of two. 32-34 Further, the redox potential of the two pseudosymmetrical phylloquinones (Figure 1B) vary significantly. 35, 36 This results in both forward and reverse electron transfer rates that differ by a factor of ten for the phylloquinones in the two branches.<sup>32, 37</sup> In the case of Type II RCs this is pushed to the extreme, with electron transfer exclusively in the A-branch and back reaction lifetimes of the two quinones that differ by several orders of magnitude.<sup>38</sup>

Regardless of the type of RC, the combination of six (B)Chls/(B)Pheo molecules that are present in the RC core are ultimately responsible for light-driven charge separation and the early steps of electron transfer. In fact, the only cofactors used for charge separation within photosynthetic RCs are (B)Chls, which is largely ascribed to the versatility of these molecules. However, while it is known that (B)Chl molecules initiate charge separation, the mechanism is not well understood in many RCs because the initial steps, which occur on an ultrafast (fs – ps) time scale, are faster than the energy transfer and involve molecules with very similar optical properties, rendering it difficult to deconvolute the different processes. Several models for charge separation have been proposed in the literature that can broadly be classified into three categories: (i) Photoexcitation of the primary donor,  $P_{\lambda}$ , and direct electron transfer from  $P_{\lambda}$ , to an

acceptor,  $A_i^{39-45}$  (ii) photoexcitation of (B)Chl<sub>2</sub>, leading to reduction of (B)Chl<sub>3</sub> or (B)Pheo, and oxidation of the resulting (B)Chl<sub>2</sub>• anion by  $P_{\lambda}$ ; <sup>46-50</sup> and (iii) photoexcitation of a tetramer or hexamer composed of the early (B)Chls. <sup>51-56</sup> Regardless of the mechanism, the first (meta)stable charge-separated state (i.e. with a lifetime > 10 ps) involves transfer of an electron from  $P_{\lambda}$  to (B)Chl<sub>3</sub> or (B)Pheo. Here, we will use the spectroscopic notation  $P_{\lambda}^{\bullet+}A_0^{\bullet-}$  for this state. It should be noted, however, that  $A_0$ , much like  $P_{\lambda}$ , is a spectroscopic term not necessarily associated with any specific crystallographic label, and throughout this chapter we will use  $A_0$  to refer to the electron acceptor in the first metastable charge-separated state.

Optical spectroscopy has been extensively used to study the primary donor and acceptor of both Type I and Type II RCs. Historically, optical studies of the primary acceptor were difficult due to the short-lived nature of the  $A_0^{\bullet-}$  state and severe spectral congestion resulting from the variety of pigments that are present in RCs. However, there are exceptions for both Type I and Type II RCs. The most easily studied RCs are those of purple bacteria because they can be isolated separately from the antenna complexes and the co-factors involved in the initial charge separation are all spectroscopically distinct. Early optical studies of the bRC revealed that BPheo and BChl molecules were readily distinguishable in vivo by absorbance changes at 762 nm/542 nm and 802 nm/590 nm, respectively. 57-59 From the absorbance characteristics, it was clear that the primary acceptor was a monomeric BPheo molecule, which was in excellent agreement with the subsequent high-resolution X-ray crystal structures of the bRC. 1, 60 However, the X-ray crystal structures also revealed the presence of a BChl molecule (BChl<sub>2A/2B</sub>) located between the primary donor, BChl<sub>1A/1B</sub>, and BPheo acceptor, and the distance between the latter two was too far for fast and efficient electron transfer. The advent of optical techniques with greater temporal resolution, coupled with targeted cofactor replacement, allowed for the direct detection of the transient intermediate, BChl<sub>2</sub>•-61-69 However, in each case it was theorized that these cofactors functioned independently as monomers. Subsequent EPR spectroscopy studies confirmed this model, where the analysis of electron-nuclear hyperfine coupling constants for the Pheo • state in the bRC matched those of the monomeric Pheo anion in vitro. 70, 71 Analogous results were also observed for the Type II RC, Photosystem II (PSII). While the studies of PSII revealed an identical pattern with a Pheo molecule (Pheo<sub>A</sub>) functioning as the first stable electron acceptor, they also showed that Chl<sub>2A</sub> acts as the origin of charge separation, which was in stark contrast to the bRC. 72, 73

The primary electron transfer pathway of the Type I RC from *Heliobacterium modestacaldum* (HbRC) can also be resolved by optical spectroscopy because it is 8-OHChl a, while all other pigments in the HbRC are BChl g or BChl g'. However, because both the antenna Chls and electron transfer cofactors are bound to the HbRC core the site of the initial charge separation has yet to be determined conclusively in HbRCs. Virtually all early studies of the primary acceptor of Type I RCs were performed on PSI, using optical spectroscopy; pump-probe experiments with picosecond time resolution. A comparison of the spectra acquired at 150 ps and 800 ps after photoexcitation revealed a 30 nm red-shifted Chl a anion peak, centered at 695 nm, that was attributed to reduction of a Chl acceptor that was proposed to be a dimer, in contrast with the monomeric primary (B)Pheo acceptor that was observed in the Type II bacterial RC (bRC) from *Rhodobacter (Rba.) sphaeroides*. Under strongly reducing conditions at a potential of -625 mV, achieved using various reducing agents, the light-minus-dark spectra displayed bleaching at 425 nm, 450 nm, and 700 nm, with a lifetime of  $\sim 1$  ms which was also suggested to be due to the presence of a reduced Chl a dimer. The transfer of the presence of a reduced Chl a dimer. The transfer of the presence of a reduced Chl a dimer. The transfer of the presence of a reduced Chl a dimer. The transfer of the presence of a reduced Chl a dimer. The transfer of the presence of a reduced Chl a dimer. The transfer of the presence of a reduced Chl a dimer. The transfer of the presence of a reduced Chl a dimer. The transfer of the presence of a reduced Chl a dimer. The transfer of the presence of a reduced Chl a dimer.

Subsequently, EPR spectroscopy was employed to study the  $A_0^{\bullet-}$  state of PSI, trapped by cryogenic photoaccumulation under strongly reducing conditions. Interestingly, initial EPR studies suggested that  $A_0^{\bullet}$  was a monomeric Chl, which was at in contrast with previous optical spectroscopy data. 82 Heathcote and coworkers sought to trap the  $A_0^{\bullet}$  state through high light treatment of PSI,82 which resulted in the observation of EPR signals with a line width of 14 G, which was larger than the 7.5 G of the well-known dimeric Chl, P<sub>700</sub>. 83, 84 Similar results were also obtained by Fajer and coworkers who used both continuous-wave (CW) EPR and electron nuclear double resonance (ENDOR) spectroscopy to study the primary acceptors of both PSI and PSII. 85, 86 The differences in the nature of the primary acceptor of PSI in the two studies were attributed to differing preparations and experimental conditions. However, it is important to note that the presence of the A<sub>1</sub> phylloquinone acceptor (Figure 1B) was not recognized at the time that this work was performed. Given the relative ease of photoaccumulating the A<sub>1</sub> • state relative to  $A_0^{\bullet-}$  and the similar g-values and line widths of the  $A_1^{\bullet-}$  and monomeric Chl  $a^{\bullet-}$ anion signals in vitro using X-band EPR spectroscopy, 84, 87 it appears that researchers were detecting the first EPR spectra of the photoaccumulated A<sub>1</sub>•- state. One feature that was not observed were the partially resolved hyperfine features associated with the A<sub>1</sub><sup>•-</sup> state at X-band frequency.87

More recently, we examined the A<sub>0</sub><sup>•</sup> state of PSI by employing a combination of twodimensional (2D) hyperfine sublevel correlation (HYSCORE) and density functional theory (DFT) methods. 88, 89 Here, the photoaccumulation of the  $A_0^{\bullet-}$  state was achieved by illuminating PSI preparations that were lacking the electron acceptor A<sub>1</sub> (Figure 1B). This was achieved in three ways: (i) by chemical extraction of the A<sub>1</sub> acceptor, (ii) by interruption of the biosynthetic pathway of phylloquinone molecules in the A<sub>1</sub> acceptor site by inactivation of the menB gene, which codes for a 1,4-dihydroxy-2-naphthoate synthase, 90-93 and (iii) the alteration of the axial ligand of the  $Chl_{3A}$  cofactor from a  $Met688_{PsaA}$  to  $His688_{PsaA}$  residue. In the first two cases, the lack of the  $A_1$  acceptor creates a longer inter-cofactor distance of approx. 25-30~Å between  $A_0$ and the next electron acceptor, Fx, resulting in charge recombination being favored over forward electron transfer. 81, 94, 95 In the case of genetic alteration of the axial ligand, the change in redox potential of  $Chl_{3A}$  that accompanies a change in the axial ligand from  $Met688_{PsaA}$  to  $His688_{PsaA}$ causes electron transfer to be blocked in  $\sim 50\%$  of PSI complexes along the A branch of electron transfer. 96 All three of the PSI preparations resulted in the photoaccumulation of the A<sub>0</sub> - state that allowed for 2D <sup>14</sup>N HYSCORE measurements revealing electron delocalization over multiple Chl a molecules. Moreover, DFT calculations of computational models derived from the X-ray crystal structure of PSI<sup>2</sup> indicated that the unpaired electron spin density was indeed delocalized over both Chl<sub>2A</sub> and Chl<sub>3A</sub> in the A<sub>0</sub>•- state. 88, 89 Interestingly, the only difference between the methods of sample preparation, namely, extraction or biosynthetic interruption of the A<sub>1</sub> phylloquinone or mutation of the axial ligand of Chl<sub>3A</sub>, was in the extent of the electron spin delocalization on the individual Chl rings. In PSI lacking the A<sub>1</sub> acceptor, the ratio of the electron spin density distribution on the Chls in the  $A_0^{\bullet}$  state was ~ 1:3::Chl<sub>2</sub>:Chl<sub>3</sub>. However, when the energetics were altered by mutation of the axial ligand of Chl<sub>3A</sub> from Met to His, the ratio was ~ 3:1::Chl<sub>2</sub>:Chl<sub>3</sub>.<sup>89</sup> These experiments provided definitive evidence that A<sub>0</sub> acceptor of PSI was a composed of a dimer of Chl<sub>2</sub> and Chl<sub>3</sub>, which is qualitatively analogous to the primary donor, P<sub>700</sub>, which is also contains dimeric Chl a molecules.

This finding that the  $A_0$  acceptor of PSI is composed of a dimer of  $Chl_2$  and  $Chl_3$  has inspired us to attain a better understanding of the principles that govern the high efficiency of charge separation as well as the protein matrix effects that control the energetics and dimerization of primary electron acceptors in a variety of RCs. In this review, we examine the primary acceptor of five different RCs with representative examples from both Type I and Type II RCs.

Table I.	Photosystem I (PSI)		
Residue	Distance (Å)	Nearest Cofactor	Notes
Met688 <sub>PsaA</sub>	2.6	Chl <sub>3</sub>	Axial Ligand
Tyr696 <sub>PsaA</sub>	2.7	Chl <sub>3</sub>	Hydrogen (H)-Bond
Water	1.9	$Chl_2$	Axial Ligand
		r Bacterial RC (Gsb	oRC)
Residue	Distance (Å)	Nearest Cofactor	Notes
Arg502	3.4	Chl <sub>3</sub>	
Ser637	3.2	Chl <sub>3</sub>	
Met429	3.1	Chl <sub>3</sub>	
Trp550	3.4	Chl <sub>3</sub>	
Phe495	4.6	Chl <sub>3</sub>	
Ala626	3.5	Chl <sub>3</sub>	
Lys553	3.0	$Chl_2$	Axial Ligand
Tyr440	2.7	$Chl_2$	H-Bond
Phe625	3.3	$Chl_2$	$\pi$ -stacked
	Helioba	ncterial RC (HbRC)	
Residue	Distance (Å)	Nearest Cofactor	Notes
Arg406	3.2	Chl <sub>3</sub>	
Ser553	2.7	Chl <sub>3</sub>	H-Bond
Ser545	3.2	Chl <sub>3</sub>	
Leu451	3.9	Chl <sub>3</sub>	
Phe548	3.3	Chl <sub>3</sub>	
Phe455	3.4	Chl <sub>3</sub>	
Phe399	4.1	Chl <sub>3</sub>	
Phe542	3.9	Chl <sub>3</sub>	
Water	2.5	Chl <sub>3</sub>	Axial Ligand/Water Pool
Water	3.6	Chl <sub>3</sub>	Water Pool
Water	4.0	Chl <sub>3</sub>	Water Pool
Trp540(A)	3.6	$Chl_2$	
Trp540(B)	3.9	$Chl_2$	
Ala541	3.4	$Chl_2$	
Gln458	3.4	$Chl_2$	
Tyr510	2.8	$Chl_2$	H-Bond
Water	2.7	$Chl_2$	Axial Ligand

Water 2.7 Chl<sub>2</sub> Axial Ligand Representing Type I RCs, we analyze cyanobacterial PSI<sup>2</sup>, the RC from *H. modestacaldum* (HbRC),<sup>5</sup> and the green sulfur bacterial RC (GsbRC) from *Chlorobaculum tepidium*.<sup>4</sup> For Type II RCs, we examine PSII<sup>3</sup> and the bRC from *Rba. sphaeroides*.<sup>1</sup> Herein we provide a detailed comparison of the geometric structures of these primary acceptors as observed in the respective high-resolution structures, including the amino acid residues and water molecules that constitute the (B)Chl and (B)Pheo binding pocket. In parallel, we analyze the electronic structure of each

primary acceptor, including the impact of the smart matrix effects of the surrounding protein environment using DFT methods to model the reduced acceptor state.

## Geometric Structure of the Primary Acceptors of Type I Reaction Centers

All known Type I RCs share the same general architecture of their polypeptides and electron

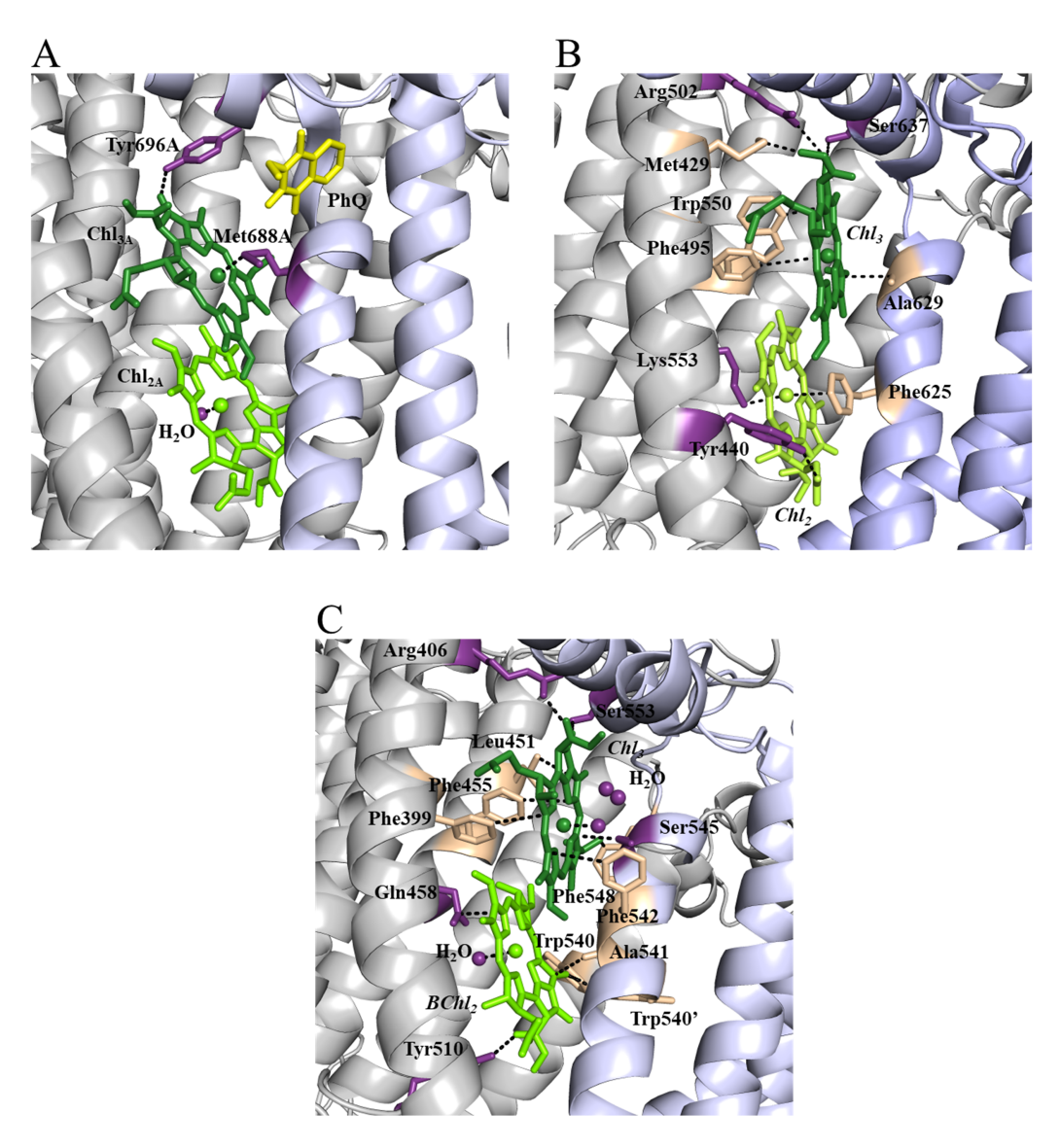


**Figure 3**. Binding pocket of the Chl<sub>2</sub>/Chl<sub>3</sub> (light green/dark green) dimer from **(A)** Photosystem I (PSI),<sup>2</sup> **(B)** GsbRC,<sup>4</sup> and **(C)** HbRC.<sup>5</sup> Different subunits composing the transmembrane are colored gray and light blue. Polar or H-bonding residues, and axial ligands are depicted in purple, while non-polar residues are shown in peach.

transfer cofactors.<sup>2, 4, 5</sup> The early electron donor and acceptor that are involved in charge separation are comprised of six (B)Chl molecules. These molecules are arranged in three pseudo-

symmetric pairs (B)Chl<sub>1A</sub>(B)Chl<sub>1B</sub>, (B)Chl<sub>2A</sub>(B)Chl<sub>2B</sub>, and (B)Chl<sub>3A</sub>(B)Chl<sub>3B</sub>. In every known Type I RC, the (B)Chl<sub>1A</sub>(B)Chl<sub>1B</sub> and (B)Chl<sub>2</sub>(B)Chl<sub>3</sub> pairs adopt a similar dimeric motif maintaining the same relative orientation of the molecules. In all cases, both branches converge at a [4Fe–4S] cluster termed F<sub>X</sub>. Subsequent electron transfer occurs to a two [4Fe–4S] cluster ferredoxin that may be tightly or loosely bound. Despite the general similarities, there are nuanced and important differences in both the chemical composition of the (B)Chls, lifetimes and energetics involved in electron transfer, and even in the presence or absence of additional acceptor molecules. Below we will discuss each RC in greater detail.

#### Photosystem I

Cyanobacterial Photosystem I (PSI) is a heterodimeric Type I RC, containing 12 or 13 polypeptide subunits, which functions as an oxidoreductase capable of oxidizing a cytochrome or plastocyanin and reducing a ferredoxin or flavodoxin.<sup>31</sup> The electron transfer cofactors,  $P_{700}$ ,  $A_0$ ,  $A_1$  and  $F_X$ , are bound within the trans-membrane polypeptides, PsaA and PsaB, in the core of PSI, while the terminal acceptors are bound in the stromal polypeptide, PsaC (**Figure 1A-B**). The electron transfer chain is composed of six Chl a (Chl<sub>1A/1B</sub>, Chl<sub>2A/2B</sub> and Chl<sub>3A/3B</sub>) and two phylloquinone ( $A_{1A/1B}$ ) molecules arranged in two pseudo-symmetric branches, termed A and B. Earlier studies have demonstrated that the two branches are not used equally, with the A-branch being employed approximately two times more than the B-branch<sup>32, 33, 97</sup> and the rates of electron transfer along the two branches are different as well.<sup>32, 34</sup> These two branches of electron transfer through the core of PSI merge at  $F_X$ , which is an inter-polypeptide [4Fe–4S] cluster bound between the PsaA and PsaB polypeptide. Subsequently, the electron is transferred to the terminal [4Fe–4S] clusters,  $F_A$  and  $F_B$ , bound within PsaC. For details on the lifetime of each of these electron transfer events, please see (31, 34).<sup>31, 34</sup>

Illumination of PSI results in the photoexcitation of  $P_{700}$  and rapid formation of a charge-separated state within  $\sim 100$  fs among the six core Chl a molecules. While the precise mechanism of charge separation is still under investigation, the first stable state,  $P_{700}^{\bullet+}A_0^{\bullet-}$ , is formed between two pairs of Chl dimers,  $P_{700}$  (a dimer of Chl<sub>1</sub>/Chl<sub>2</sub>) and  $A_0$  (a dimer of Chl<sub>2</sub>/Chl<sub>3</sub>). Analysis of the structural features of the Chl<sub>2A/3A</sub> pair that comprises the  $A_{0A}$  acceptor reveals a high degree of similarity to the primary donor,  $P_{700}$ , of PSI. A depiction of the structure is presented in Figure 3A, with the important distances and structural features listed in

Table 1. Briefly, there is a single hydrogen bond to Chl<sub>3A</sub> provided by the Tyr696<sub>PsaA</sub> residue and the axial ligands to Chl<sub>3A</sub> and Chl<sub>2A</sub> are the Met688<sub>PsaA</sub> residue and a water molecule, respectively. Note that for PSI we have kept the amino acids in the binding site relatively simple in comparison to the other RCs we analyzed in this study, as the recapitulation of experimental hyperfine parameters was possible while including the cofactors and amino acids mentioned above.<sup>88</sup>

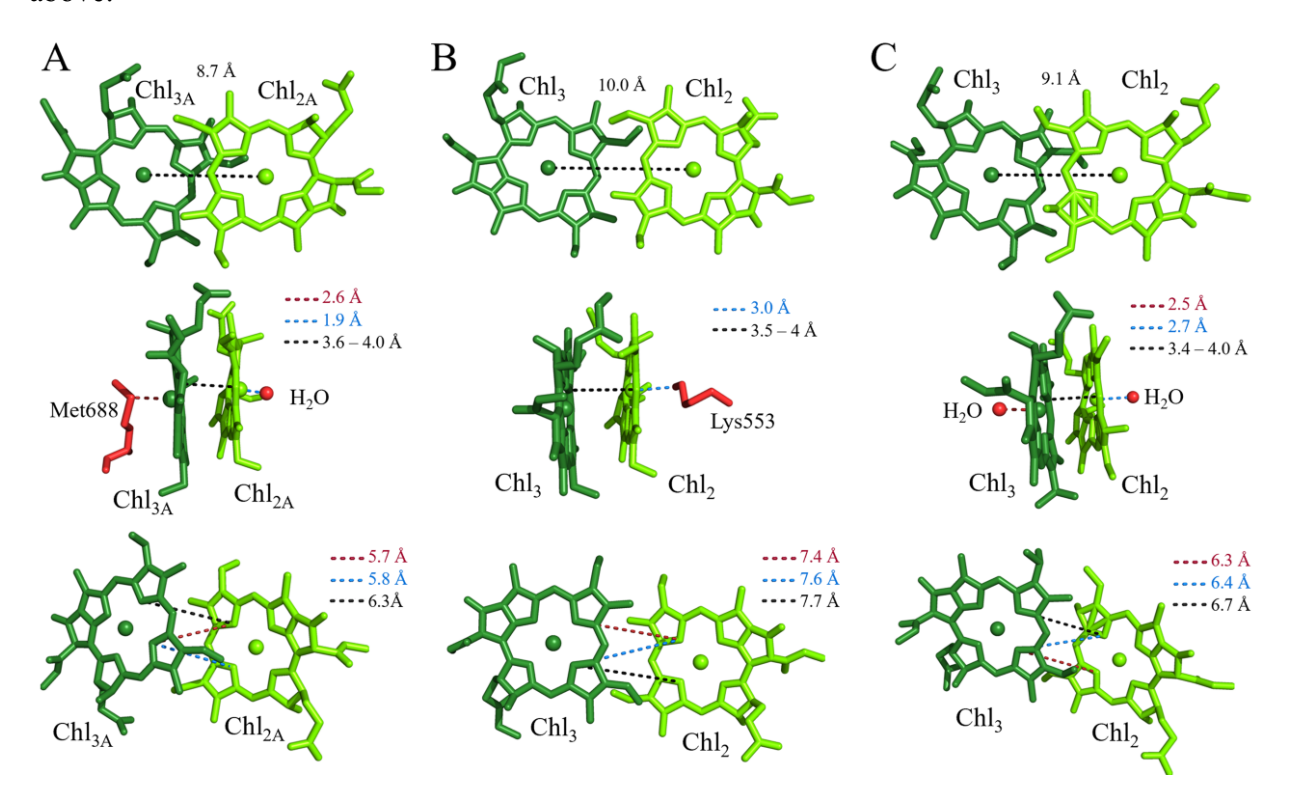


**Figure 4**. Comparison of the structure, relative orientation and inter-atomic distances of the Chl<sub>2</sub>/Chl<sub>3</sub> pairs in **(A)** PSI,<sup>2</sup> **(B)** GsbRC,<sup>4</sup> and **(C)** HbRC.<sup>5</sup>

Shown in **Figure 4A** are the inter-cofactor distances between the  $Chl_{3A}$  and  $Chl_{2A}$  rings of the  $A_{0A}$  acceptor. The Mg-Mg distance is 8.7 Å, which is the shortest of all the Type I RCs with known structures. Interestingly, it is approx. 3.4 Å longer than the inter-cofactor distance between the  $Chl_{1A/1B}$  molecules in  $P_{700}$ , but still results in significant overlap of  $Chl_{3A}$  and  $Chl_{2A}$ , which remain in a  $\square$ -stacked orientation. The distance between the ring planes varies from 3.6 – 3.9 Å, which is comparable to that of  $P_{700}$ . Perhaps the biggest deviation from  $P_{700}$  is in the identity and distance between the nearest ring nitrogen atoms. In  $P_{700}$ , the  $N^3$  nitrogen from  $Chl_{1A}$  is proximal to the  $N^3$  nitrogen of  $Chl_{1B}$  (3.6 Å), while in  $A_0$ ,  $N^3$  of  $Chl_{3A}$  is proximal to both the  $N^3$  and  $N^2$  nitrogens of  $Chl_{2A}$ , at distances of 5.8 Å and 5.7 Å, respectively.<sup>2,88</sup>

## Green Sulfur Bacterial Reaction Center (GsbRC)

The GsbRC from C. tepidum is similar to PSI, albeit with several important differences. The electron transfer cofactors of the GsbRC are also bound within three distinct subunits: two within the membrane (PscA), and one located on the stromal side of the membrane (PscB) (Figure 1C-D). However, while PSI is a heterodimer where the PsaA and PsaB polypeptides are encoded by different genes and have structural distinctions between them, the GsbRC is a homodimer of two identical PscA subunits. 23, 24 It should be noted that the orientation PscB does break the symmetry of the GsbRC as a whole, but the electron transfer cofactors within the homodimeric PsaA core remain symmetric. <sup>4</sup> These cofactors are comprised of two BChl a molecules, four Chl a molecules, and three [4Fe-4S] clusters. This is the first RC presented here where the identity of the early (B)Chl cofactors in the RC are not identical. The primary donor ( $P_{840}$ ) is comprised of the two BChl a molecules, while the Chl<sub>2</sub>/Chl<sub>3</sub> cofactors are Chl a molecules. The difference in the redox potential of the BChl a and Chl a molecules  $^{85, 99}$  likely impacts the energetics of both the primary charge separation and subsequent electron transfer, although the effect is not fully understood. Regardless, the two branches for electron transfer in this system are symmetric, and thus by definition both branches are accessed equally. In another significant deviation from PSI, the GsbRC lacks a quinone acceptor, A<sub>1</sub>, after Chl<sub>3</sub> (Figure 1D), and electron transfer occurs directly from the primary acceptor, A<sub>0</sub>, to the [4Fe-4S] cluster, F<sub>X</sub>. 4, 24 Subsequently, the electron is transferred to the terminal F<sub>A</sub> and F<sub>B</sub> clusters located in the loosely bound PscB polypeptide subunit.

In turning our attention to the  $Chl_2/Chl_3$  pair in the GsbRC, we find that even though its  $A_0$  cofactor shares the general structure and orientation common to other Type I RCs, it has several unique aspects. First, the inter-cofactor distance between the central  $Mg^{2+}$  ions of  $Chl_2$  and  $Chl_3$  is longer at 10.0 Å (Figure 4B). In fact, this is the longest distance among all Type I RCs with published structures. An obvious consequence is that there is a similar increase in the distance to the nearest ring nitrogen atoms. This increase in the distance between the  $Chl_2$  and  $Chl_3$  molecules, however, is not mirrored in the distance between ring planes, which remains at  $\sim 3.5$  Å, well within the range distances observed in PSI ( $\sim 3.6$  Å) and HbRC ( $\sim 3.3$  Å). Thus, while we anticipate a weaker coupling of  $Chl_2$  and  $Chl_3$  pair in the  $A_0$  state, we still expect dimerization of the acceptor in the GsbRC.

The A<sub>0</sub> binding site of the GsbRC (**Figure 3B**) also has aspects that differentiate it from other Type I RCs and likely help tune its redox properties. The axial ligand to the central Mg<sup>2+</sup> ion of Chl<sub>3</sub> is presumed to be a water molecule, even though it is not resolved in the cryo-electron microscopy (EM) structure, making it identical to that of the HbRC.<sup>5</sup> However, Chl<sub>2</sub> contains a lysine residue, Lys553<sub>PscA</sub>, as an axial ligand (located within 3.0 Å of the central Mg<sup>2+</sup> ion). This makes it the only Type I RC with an A<sub>0</sub> ligand chemistry most closely aligned with the accepted rules for hard-soft acid-base theory, where the relatively hard acid, Mg<sup>2+</sup>, is ligated by a hard base nitrogen atom from a lysine residue. Moreover, this deviates from all of the other known Type I RCs, where the axial ligand of Chl<sub>2</sub> is a water molecule. In terms of hydrogen bonds, it appears that two residues form weak hydrogen bonds to Chl<sub>3</sub>, namely, Gln645<sub>PscA</sub> and Arg502<sub>PscA</sub>, that are located within a distance of 3.6 and 3.4 Å, respectively. Interestingly, the interactions with both residues appear in the same quadrant of the Chl containing the cyclopentanone group and Chl<sub>2</sub> has only a single strong hydrogen bond to Tyr440<sub>PscA</sub>.

Perhaps the most unexpected feature of this binding site is the presence of a phenylalanine residue (Phe625<sub>PscA</sub>) that appears to be  $\square$ -stacked with Chl<sub>2</sub> with a distance of 3.3 Å between the two rings (**Figure 3B**). This residue appears analogous to Trp697<sub>PsaA</sub>/Trp677<sub>PsaB</sub> in PSI, which serve to drive the redox potential of the A<sub>1</sub> phylloquinone to a more negative value. This is the only RC where this motif is clearly observed for a Chl or Pheo molecule in either a Type I or Type II RC, respectively. While several Phe and other aromatic groups line the binding pocket of A<sub>0</sub> from both PSI and HbRC, none of these are observed in a  $\square$ -stacked orientation. The complete list of amino acids interacting with the Chl<sub>2</sub> and Chl<sub>3</sub> molecules are presented in **Table 1**.

### Heliobacterial Reaction Center (HbRC)

The HbRC is arguably the simplest of all the Type I RCs. The electron transfer cofactors are contained in a homodimer of PshA subunits<sup>5, 100, 101</sup> (**Figure 1E-F**) (analogous to PscA and PsaA/PsaB polypeptides of the GsbRC and PSI, respectively). The HbRC clearly lacks a terminal PscB/PsaC-type polypeptide subunit with terminal electron acceptors, instead relying on a series of mobile ferredoxins.<sup>101</sup> The primary pigment of the HbRC is BChl *g*, which constitutes both the antenna system and a majority of the early Chl acceptors. Similar to the GsbRC, the electron transfer pathway of the HbRC bifurcates into two branches, containing a primary donor

(P<sub>800</sub>), and two pairs of (B)Chl molecules that constitute  $A_0$ . Again, as these branches are symmetric, it is assumed that they have similar rates of electron transfer and are used equally. The branches then converge and terminate at the [4Fe–4S] cluster,  $F_X$  (Figure 1F).

The Chl<sub>2</sub> and Chl<sub>3</sub> binding pocket of the HbRC share few similarities to  $A_0$  of PSI, in the form of a similar hydrogen bond to the same carbonyl moiety in Chl<sub>3</sub> (**Figure 3C**). However, while  $A_0$  in PSI appears to be a pseudo-homodimer of Chl a molecules bound within a RC with a heterodimeric polypeptide core,  $A_0$  in the HbRC is a heterodimer of (B)Chl molecules bound within a RC with a homodimeric core.<sup>5</sup> This is readily seen in the identity of the (B)Chl molecules that compose the  $A_0$  acceptor; Chl<sub>2</sub> is a BChl g (the primary Chl pigment found in the RC), and Chl<sub>3</sub> is an  $8^1$ -OH-Chl a, meaning that the dimer is composed of two different types of (B)Chls. The implications of this heterodimerization is not obvious, since there is a lack of experimental data determining the redox properties of BChl g, as compared with Chl a, Chl b, and Chl a pigments. However, it seems likely that this will significantly impact the delocalization and may even be the primary factor in controlling the redox potential difference and asymmetry in electron transfer.

Taking steps to alleviate any strain caused by this heterodimerization of (B)Chl cofactors may be manifested in the other differences to PSI; namely, the presence of a hydrogen bond to Chl<sub>2</sub>, and the identity of the axial ligands. There is a second hydrogen bond to a carbonyl group of Chl<sub>2</sub>, provided by Tyr510<sub>PshA</sub> (Figure 3C), that is not present in PSI. It should be noted that there is an analogous hydrogen bond in Chl<sub>3</sub>, implying that the hydrogen bonding interactions may have a similar effect on the redox potential of both Chls. The axial ligand will also similarly impact each Chl, as each of them is coordinated by a water ligand. This is important as changing the identity of the axial ligand of the Chl has been demonstrated to have a significant effect on electron transfer<sup>96</sup> and the asymmetry of electron delocalization over the A<sub>0</sub> dimer in PSI.<sup>89</sup> This suggests that the most significant protein matrix effects are impacting the redox properties of both Chls in the same manner, roughly balancing them and ensuring that any asymmetry in electron delocalization is driven by the differential identity of the Chl molecules. A noteworthy aspect of the A<sub>0</sub> binding site of the HbRC is the number of amino acids interacting with the BChl<sub>2</sub>/Chl<sub>3</sub> pair (Figure 3C). The majority of these are aromatic residues that appear to serve as structural components, likely ensuring preferential binding of the 8<sup>1</sup>-OH-Chl a. Interestingly,

this contrasts with the binding site of the primary donor,  $P_{800}$ , which has remarkably few interacting residues.<sup>22</sup> Table 1 provides more details on the  $A_0$  binding site of the HbRC.

The  $A_0$  cofactor of the HbRC, however, does share a high similarity to  $A_0$  of PSI in terms of inter-cofactor distance and orientation (**Figure 4C**). The Mg-Mg distance is 9.1 Å, which is in between PSI and the GsbRC, and corresponds to a marginally longer distance between the nearest nitrogen atoms of the neighboring rings. While the ring overlap is not as extensive, given the longer Mg-Mg distance, the distance between the ring planes varies from 3.3 to 3.6 Å, and is comparable to PSI. As such, from a structural perspective we would expect that this (B)Chl pair would retain some amount of delocalization across both rings.

## **Geometric Structure of the Primary Acceptors of Type II Reaction Centers**

We now turn our attention to the primary acceptor system of Type II RCs. Similar to Type I RCs, all Type II RCs adopt the same general archetype for their electron transfer cofactors. Four core (B)Chls comprise the early donor-acceptor system, with (B)Chl<sub>1A</sub>/(B)Chl<sub>1B</sub>, (B)Chl<sub>2A</sub>/(B)Chl<sub>2B</sub> forming two pseudo-symmetric pairs. This is followed by the pseudo-symmetric pairs of Pheo<sub>A</sub>/Pheo<sub>B</sub>, as well as quinones Q<sub>A</sub>/Q<sub>B</sub>. Differences between Type I RCs are apparent both in cofactor identity and their cofactor positioning. As mentioned above, not only is this system composed of a (B)Chl and Pheo, but the relative orientation of these two cofactors are significantly different than that of Type I RCs. Below we will provide more detailed information on the Type II RCs of the bRC and PSII.

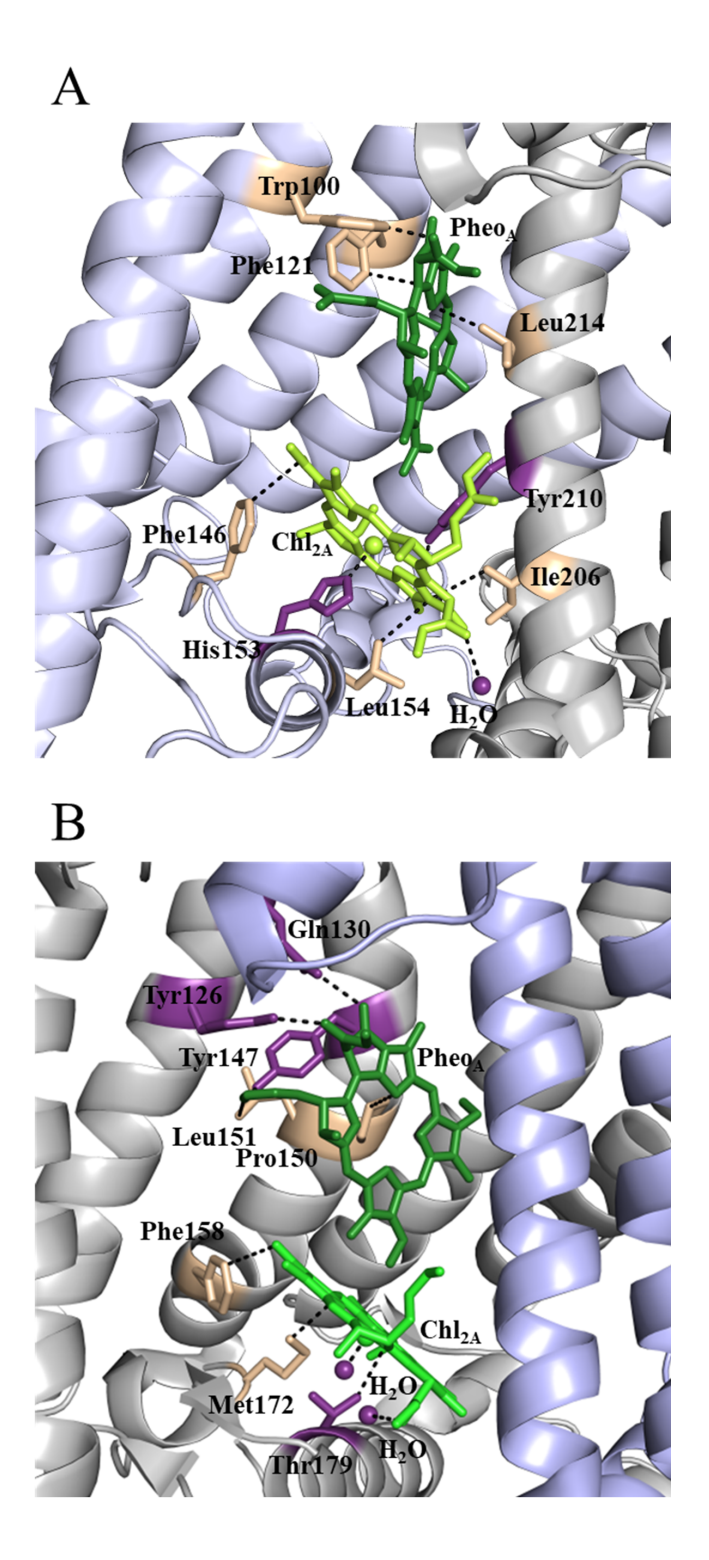


**Figure 5.** Binding pocket of the Chl<sub>2A</sub>/Pheo<sub>A</sub> (light green/dark green) from **(A)** the bRC from *Rba*. sphaeroides<sup>1</sup> and **(B)** Photosystem II (PSII).<sup>3</sup> Different subunits composing the trans-membrane helices of the core polypeptides are colored white and light blue and the polar or hydrogen bonding residues, and axial ligands are depicted in purple, while non-polar residues are shown in peach.

#### **Bacterial Reaction Centers**

The bRC from *Rba. sphaeroides* (**Figure 2A**) is composed of three polypeptide subunits, L, M, and H, with the electron transfer cofactors being housed in the L and M subunits (**Figure 2A**). In the electron transfer chain begins at the primary donor, P<sub>865</sub>, a dimer of BChl a molecules, BChl<sub>1A</sub> and BChl<sub>1B</sub>. Proximal to the P<sub>865</sub> BChls are a pair of nearly symmetrically structured BChl a molecules that compose the accessory BChls: BChl<sub>2A</sub> and BChl<sub>2B</sub> (**Figure 2B**). While these accessory BChls appear symmetric with respect to P<sub>865</sub>, only BChl<sub>2A</sub> is cofactor actively involved in the electron transfer pathway. Next, there are two symmetrically arranged BPheo molecules, BPheo<sub>A</sub> and BPheo<sub>B</sub> (also termed BPheo<sub>L</sub> and BPheo<sub>M</sub>, respectively), where again only the A-branch is active in electron transfer. From the BPheo, the electron is transferred to the primary and secondary quinone acceptors, Q<sub>A</sub> and Q<sub>B</sub>. Unlike the Type I RCs described in the previous section, whose function can be completed with a single turnover, the Type II RCs require two-electron and two-proton turnovers to doubly reduce Q<sub>B</sub> to the quinol, O<sub>B</sub>H<sub>2</sub>. St. 105-109

The binding pocket of the BChl<sub>2A</sub>/BPheo<sub>A</sub> pair in the bRC is relatively simple, with significantly more aromatic and non-polar residues than polar and hydrogen bonding residues (**Figure 5A**). Indeed, only a single Tyr210<sub>M</sub> residue and water molecule are in close proximity to BChl<sub>2</sub>. The three remaining aromatic residues, Phe146<sub>L</sub>, Trp100<sub>L</sub>, and Phe121<sub>L</sub> interact with the periphery of the BChl macrocycles and likely serve as structural components. However, one interesting facet of the BChl<sub>2A</sub> binding site is the axial His153<sub>L</sub> ligand. While His is a common ligand to (B)Chl molecules in RCs, and can help identify possible (B)Chl binding sites, it is often relegated to (B)Chl molecules in the antenna proteins and the primary donor in the RC. This is the first instance of any (B)Chl of the A<sub>0</sub> acceptors being natively coordinated by an axial His ligand. As mentioned above, this likely serves to lower the redox potential relative to the surrounding cofactors, impacting both primary charge separation and forward electron transfer.

Table II.	Bacterial RC (Rba. sphaeroides)				
Residue	Distance (Å)	Nearest Cofactor	Notes		
Trp100	3.0	Pheo <sub>A</sub>			
Phe121	3.4	$Pheo_A$			
Leu214	3.1	$Pheo_A$			
Ile206	3.7	$\mathrm{Chl}_{2\mathrm{A}}$			
Tyr210	3.8	$\mathrm{Chl}_{2\mathrm{A}}$			
His153	2.3	$\mathrm{Chl}_{2\mathrm{A}}$	Axial Ligand		
Leu154	3.6	$\mathrm{Chl}_{2\mathrm{A}}$			
Phe146	3.8	$\mathrm{Chl}_{2\mathrm{A}}$			
Photosystem II					
Residue	Distance (Å)	Nearest Cofactor	Notes		
Tyr126	2.6	$Pheo_A$	H-Bond		
Gln130	2.9	$Pheo_A$	H-Bond		
Ile143	4.3	$Pheo_A$			
Tyr147	2.0	$Pheo_A$			
Pro150	3.5	$Pheo_A$			
Leu151	7.2	$Pheo_A$			
Phe158	3.9	$Chl_{2A}$			
Met172	3.6	$Chl_{2A}$			
Thr179	3.4	$\mathrm{Chl}_{2\mathrm{A}}$			
H <sub>2</sub> O	2.0	$\mathrm{Chl}_{2\mathrm{A}}$	Axial Ligand		
H <sub>2</sub> O	2.9	$\mathrm{Chl}_{2\mathrm{A}}$	H-Bond		

Experimental work investigating the role of this axial ligand was studied by Katilius et al., where the axial His153<sub>L</sub> ligand was replaced by a series of other amino acid residues: Asp, Gln, Glu, Gly, Leu, Phe, Ser, Val, and Tyr. These alterations resulted in a significant decrease in the rate of electron transfer from 3 ps in the wild-type bRC to 18 ps in the genetic variants, which

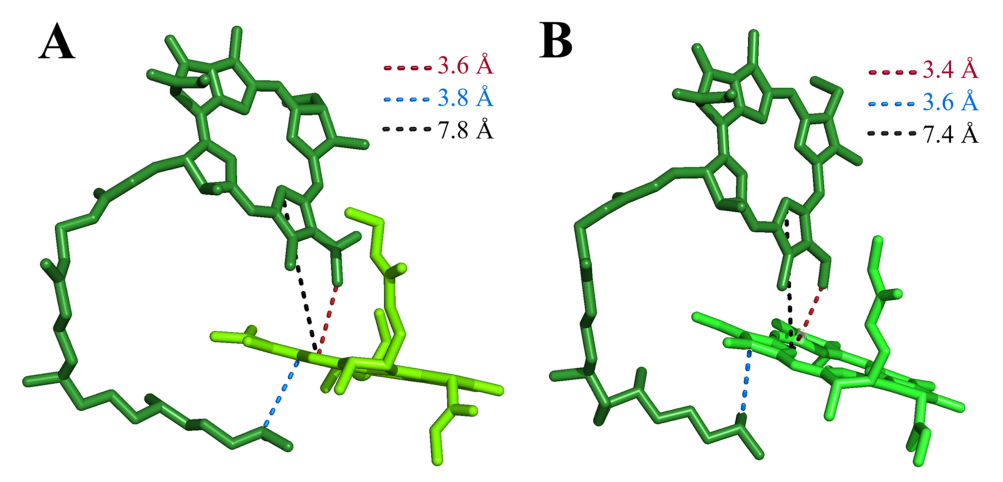


**Figure 6.** Comparison of the structure, relative orientation, and inter-atomic distances of the Chl<sub>2A</sub>/Pheo<sub>A</sub> cofactors in **(A)** the bRC from *Rba. sphaeroides*<sup>1</sup> and **(B)** PSII.<sup>3</sup>

was accompanied by a blue shift in the absorbance spectrum. For a complete list of the amino acid residues in the  $A_0$  binding site of the bRC, please refer to Table II.

#### Photosystem II

The PSII RC contains two core trans-membrane polypeptide subunits, D1 and D2<sup>3, 30</sup> (**Figure 2C-D**), analogous to L and M from the bRC, which serve to house the electron transfer cofactors. <sup>1, 60, 104</sup> However, unlike the bRC, the PSII core complex is surrounded by 22–23 smaller intrinsic and extrinsic polypeptide subunits. <sup>111, 112</sup> While the majority of cofactors involved in the primary electron transfer pathway of PSII closely resemble those of the bRC, there are two important differences. The first is the tetranuclear manganese-calcium-oxo (Mn<sub>4</sub>Ca-oxo) cluster that catalyzes the oxidation of water to dioxygen, which is one of the most energetically demanding reactions in nature. The splitting of water to dioxygen at the Mn<sub>4</sub>Ca-oxo cluster generates electrons to re-reduce the primary donor, P<sub>680</sub>, allowing for successive turnovers of the RC (**Figure 2D**). <sup>3, 112</sup> The second difference is the presence of redox-active tyrosine residues, Tyr161<sub>A</sub> (Y<sub>D</sub>) and Tyr161<sub>B</sub> (Y<sub>Z</sub>), in the core D1 and D2 polypeptides that facilitate proton-coupled electron transfer reactions that are central to the water-splitting chemistry of PSII.

In contrast to the binding pocket of the bRC, PSII has significantly more protein-matrix interaction with both the  $Chl_{2A}$  and  $Pheo_A$  cofactors (**Figure 5B**). There is an additional water molecule interacting with  $Chl_{2A}$ , one serving as an axial ligand and the other forming a putative hydrogen bond. For  $Pheo_A$ , there are three hydrogen bonding residues,  $Gln130_A$ ,  $Tyr147_A$ , and  $Tyr126_A$ , with  $Tyr126_A$  and  $Gln130_A$  interacting with the same section of the macrocycle. There are also a significant number of aromatic residues lining the binding pocket of both  $Chl_{2A}$  and  $Pheo_A$ , similar to that of the bRC. For a complete list of amino acid residues, refer to **Table II**.

As the inter-cofactor parameters for the Type II RCs, bRC and PSII, are remarkably similar, we will describe them together. Perhaps the most obvious change in the  $A_0$  acceptor of Type II RCs is the deviation of the (B)Chl molecules from the parallel orientation that was observed in Type I RCs, instead adopting a nearly orthogonal position (**Figure 6A-B**). The closest ring nitrogen atoms of  $Chl_{2A}$  and  $Pheo_A$  are those associated with  $N^{III}$  pyrrole ring that are 7.6 - 7.8 Å apart. Please note that this distance is comparable to the values observed for the  $A_0$  acceptor of the GsbRC. Moreover, the edge-to-edge distance between the rings remains reasonably close,

ranging from 3.4 - 3.8 Å. However, the aforementioned orientation precludes the overlap of  $\square$  orbitals that was observed in the Type I RCs. One rather unusual feature that is present in that  $A_0$  acceptor of both the bRC and PSII is the orientation of the tail of the Pheo<sub>A</sub> molecule, which appears to interact with the opposing side of the Chl<sub>2</sub> ring. In each case, the atoms on the tail are within 4.0 Å of the Chl molecule, and while this likely serves some purpose, its impact is unknown at this time.

## **Electronic Properties of the Reduced Primary Acceptors**

Vast strides in X-ray crystallography and cryo-EM have led to high-resolution structures of PSI, PSII, GsbRC, HbRC and bRC from thermophilic and mesophilic cyanobacteria, green sulfur bacteria, heliobacteria and purple bacteria, respectively.  $^{1-5,\ 113-117}$  As highlighted in the previous section, this has provided important information on the location and geometry of the (B)Chl and (B)Pheo cofactors in the neutral ground state of the RCs. However, these structures are lacking insight on the functional  $A_0^{\bullet-}$  state that is formed upon light-driven charge separation. Spectroscopic measurements have played a central role in determining the electronic properties of the reduced state of the individual primary acceptors. In particular, continuous-wave (CW) and pulsed EPR spectroscopy techniques are exceptionally well suited to probe the electronic structure as the high sensitivity and specificity for the detection of unpaired electron spin(s) has helped overcome limitations of the large size of the RCs, and the use of powder samples has eliminated the need for crystalline material. Therefore, both CW and pulsed EPR spectroscopy have been widely employed in the study of the charge-transfer intermediates of (B)Chl and (B)Pheo in RCs.  $^{70,\ 82,\ 83,\ 85,\ 86,\ 88,\ 89,\ 94,\ 118-126}$ 

Previous studies have demonstrated that cryogenic illumination of RCs results in the rapid formation of the charge-separated  $P^{\bullet +}A_0^{\bullet -}$  state. Subsequent re-reduction of  $P^{\bullet +}$  in the presence of exogenous electron donors allows for photo-accumulation of the reduced primary acceptor,  $A_0^{\bullet -}$ .88, 94, 126 The  $A_0^{\bullet -}$  state is paramagnetic with an unpaired electron spin, S, of ½ making it suitable for study by EPR spectroscopy. While there exist relatively few studies of the GsbRC and HbRC, PSI, the bRC from *Rba. sphaeroides* and PSII have been extensively investigated using EPR spectroscopy. The spectroscopy study on RCs demonstrated that the primary donor cation,  $P_{700}^{\bullet +}$ , of PSI<sup>83</sup>, generates a signal at a g value of 2.0025, which arises from a strongly excitonically-coupled Chl g dimer. State is paramagnetic with an unpaired electron spin, S, of ½ making it suitable for study by EPR spectroscopy. The spectroscopy is study by EPR spectroscopy.

Moreover, the line width of this signal is narrower than that of monomeric Chl  $a^{\bullet +}$  in vitro, <sup>84</sup> which provided direct evidence for the delocalization of the unpaired electron spin across the dimeric Chl<sub>1A/1B</sub> cofactors of P<sub>700</sub> • <sup>+</sup> · <sup>84</sup> Subsequently, dimerization of (B)Chls in the P<sup>+</sup> state of PSII and the bRC from *Rba*. *sphaeroides* was also demonstrated by EPR spectroscopy. <sup>138, 139</sup>

In principle, the direct measurement of magnetic electron-nuclear hyperfine couplings between the unpaired electron spin and NMR-active nuclei could reveal the distribution of the electron spin density and hence, the electronic structure of the (B)Chl<sub>2/3</sub> and (B)Chl<sub>2/4</sub>/(B)Pheo<sub>A</sub> molecules in the reduced primary acceptor,  $A_0^{\bullet-}$ . However, it is not possible to measure the hyperfine interactions using CW EPR spectroscopy due to the inhomogeneous broadening of the peaks in the spectrum. Therefore, hyperfine spectroscopy methods, such as electron nuclear double resonance (ENDOR), electron-spin-echo envelope modulation (ESEEM) and twodimensional (2D) hyperfine sub-level correlation (HYSCORE), in conjunction with computational modeling, are often used to obtain information on the electronic structure of the reduced primary acceptors. 35, 88, 89, 134, 140-148 ENDOR spectroscopy is a double resonance technique with reasonably high spectral resolution that has typically allowed for the measurement of small hyperfine couplings. 140, 141, 143, 144 Similarly, ESEEM spectroscopy has been applied to the study of paramagnetic centers in RCs as it overcomes the inhomogeneous broadening of EPR resonances and provides access to unresolved electron-nuclear hyperfine couplings. 149-151 The hyperfine couplings that are measured by ENDOR and ESEEM are orientation dependent, which means that information on the hyperfine anisotropy is lost in powder EPR samples with random orientations (e.g. frozen RC samples). Moreover, nuclear transitions of multiple abundant spins, such as, <sup>1</sup>H or <sup>14</sup>N, in powder samples or frozen samples have often been difficult to resolve by one-dimensional ENDOR and ESEEM spectroscopy due to spectral overcrowding of signals. Hence, in the past decade we and others have been employing two-dimensional (2D) hyperfine sub-level correlation (HYSCORE) spectroscopy, which is a two-dimensional version of ESEEM, used to obtain correlations between nuclear transitions, thereby facilitating the detection and assignment of multiple hyperfine-coupled proton and nitrogen atoms in two-dimensional frequency space. 11, 35, 88, 89, 134, 146, 147, 149, 151-154 All three methods are highly sensitive as the electron spin-coupled nuclear transitions are monitored through the observation of a paramagnetic electron spin. 141, 144, 155-157

In conjunction with CW and pulsed EPR spectroscopy measurements, the electronic structure of the reduced primary acceptors,  $A_0^{\bullet-}$ , of both Type I and Type II RCs, PSI, the bRC and PSII, have also been probed by semi-empirical molecular orbital, quantum mechanics/molecular modeling (QM/MM) and density functional theory (DFT) methods. This has allowed for modeling the effects of the unusual and variable axial coordination of the (B)Chls, hydrogen bonding interactions and proximity effects from the other cofactors on the  $A_0^{\bullet-}$  state in these RCs. In this section, we will describe key observations by EPR spectroscopy and DFT calculations that shed light on the electronic structure of the  $A_0^{\bullet-}$  state of both Type I and Type II RCs.

## Electronic Structure of A<sub>0</sub> in Type I Reaction Centers

As described previously, currently there are high-resolution structures available for three Type I RCs, namely, PSI, the GsbRC and HbRC.<sup>2, 4, 5</sup> The PSI RC was initially discovered in the 1950s<sup>158, 159</sup> and has since been extensively investigated by CW EPR, ENDOR, ESEEM and HYSCORE spectroscopy.<sup>83, 84, 88, 89, 153, 160-168</sup> In comparison, there are relatively limited studies on the GsbRC and HbRC.<sup>101, 169-173</sup> These studies tend to leverage knowledge on experimental methodology and results obtained from other RCs to determine the nature of the terminal [4Fe–4S] acceptors, investigate the make-up of the electron transfer chain, and characterize the primary donors.

Recently, we probed the  $A_0^{\bullet-}$  state of PSI to gain insight on the electron-nuclear hyperfine interactions with the constituent  $^1H$  and  $^{14}N$  atoms.  $^{88, 89}$  In these studies, we employed 2D HYSCORE spectroscopy as it provides enhanced resolution from the detection of hyperfine signals in two-dimensional frequency space, which eliminates overcrowding from the signals of multiple  $^1H$  and  $^{14}N$  atoms present in the  $A_0^{\bullet-}$  state.  $^{140}$  Cryogenic illumination of PSI, where forward electron transfer to  $A_1$  was inhibited and the [4Fe–4S] clusters were in the reduced state, resulted in the photoaccumulation of the  $A_0^{\bullet-}$  state.  $^{88, 89}$  We observed two sets of distinct HYSCORE signals from hyperfine interactions of the unpaired electron spin with the proximal nitrogen-14 ( $^{14}N$ , nuclear spin of I = 1) and hydrogen ( $^{1}H$ , I =  $^{1}/_{2}$ ) atoms of the  $A_0^{\bullet-}$  state in wild-type PSI.  $^{88}$  The quadrupolar coupling constant, K, obtained from quantitative analyses of the HYSCORE spectra indicated that the hyperfine couplings originated from the pyrrole nitrogen atoms of a Chl ring  $^{11, 142, 174, 175}$  and the isotropic hyperfine constants,  $A_{iso}$ , ranging from 2.8 – 0.52 MHz demonstrated that the electron spin density was distributed on at least three of the

constituent nitrogen atoms in the  $A_0^{\bullet-}$  state. Interestingly, the  $A_{iso}$  couplings of  $A_0^{\bullet-}$  were smaller than those previously reported for the <sup>14</sup>N atoms of monomeric Chl  $a^{\bullet+151}$  and Chl  $a^{\bullet-176}$  in vitro. Moreover, the couplings were similar in magnitude to those of  $P_{700}^{\bullet+}$ , indicating that the unpaired electron spin density was also delocalized over two or more Chl a rings in the  $A_0^{\bullet-}$  state.

Previous experimental work in which the axial ligand to  $Chl_{3A}$ ,  $Met688_{PsaA}$ , was changed to a hard base histidine ligand in the  $Met688His_{PsaA}$  variant had revealed severely impacted electron transfer processes at both the  $A_0$  and  $A_1$  acceptors. <sup>89, 96</sup> Using HYSCORE spectroscopy

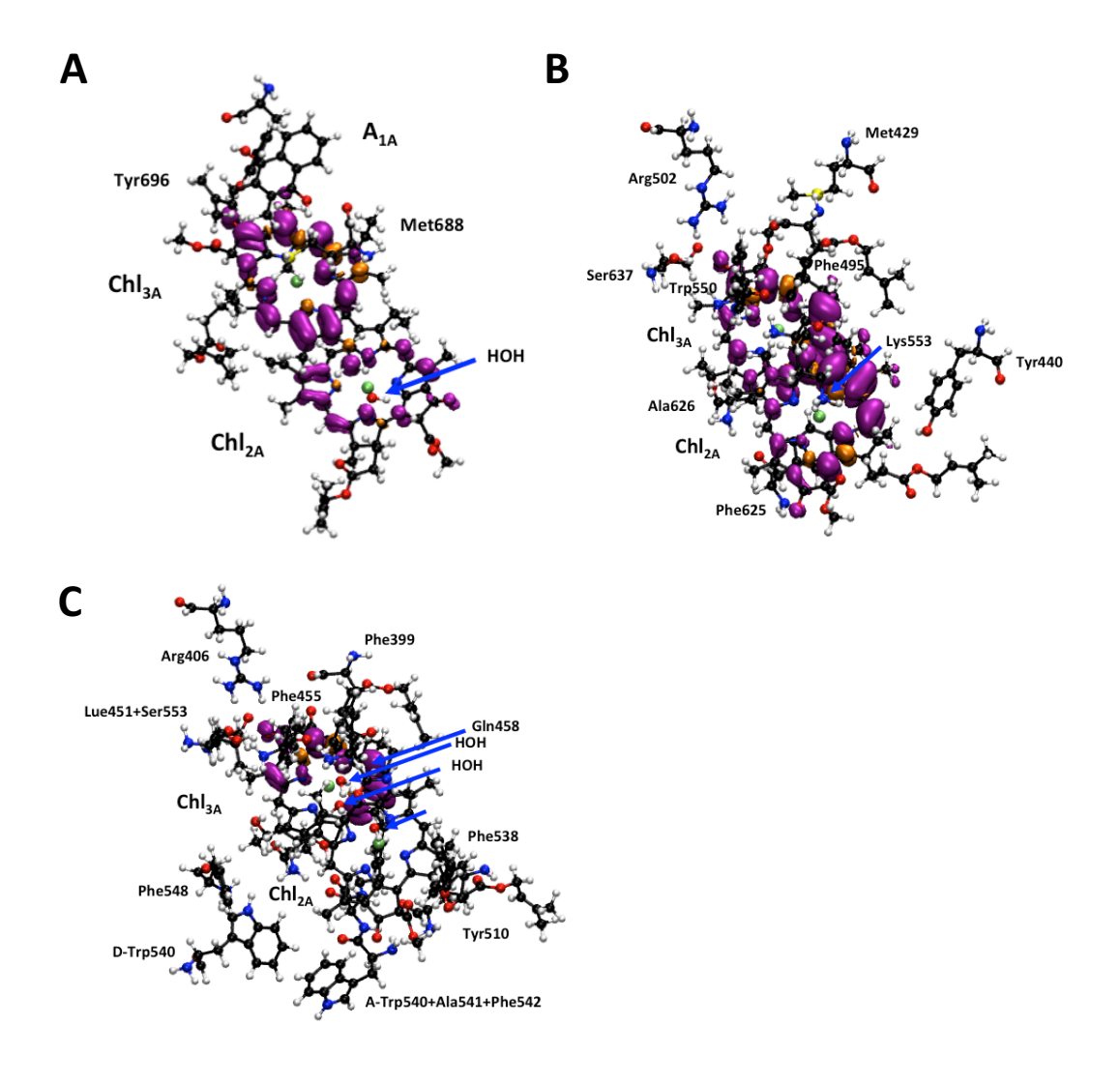


**Figure 7.** Comparison of the electronic structure of the  $A_0^{\bullet-}$  state of **(A)** PSI, **(B)** GsbRC and **(C)** HbRC based on the electron spin density distribution in the singly occupied MO on the Chl<sub>3</sub> and Chl<sub>2</sub> rings obtained using DFT methods.

measurements, we demonstrated that the imidazole side chain of His serves as an axial ligand to the central  $Mg^{2+}$  ion of  $Chl_{3A}$  in the Met688His<sub>PsaA</sub> variant of PSI and the electron spin density remains delocalized over one or more Chls in the  $A_0^{\bullet-}$  state. While delocalization of the electron spin was apparent in  $A_0^{\bullet-}$  of both wild-type and the Met688His<sub>PsaA</sub> variant of PSI, the HYSCORE spectroscopy measurements did not identify the Chl molecules that were serving as the primary electron acceptor.

We performed DFT calculations to better understand the electronic structure of the  $A_0^{\bullet-}$ state of PSI, the GsbRC and HbRC. The computational model of the primary acceptor from each RC included the (B)Chl molecules, (B)Chl<sub>2A</sub>/(B)Chl<sub>3A</sub>, the axial ligands of the (B)Chls and proximal hydrogen-bonding and hydrophobic residues in the protein matrix as observed in the respective structures (Figures 3A-C and Table I).<sup>2, 4, 5</sup> The models contained the complete BChl molecules with the exception of the phytol tail that was truncated by a methyl group after four carbon atoms. The single-point energy of each model was calculated employing the hybridgeneralized gradient approximation (hybrid-GGA) B3LYP functional along with the special EPR-optimized EPR-II<sup>180</sup> basis set for the lighter atoms and 6-31G(d) for magnesium and sulfur, respectively, for most calculations, and the valence polarization basis sets (SVP and TZVP)<sup>181-183</sup> with the decontracted auxiliary basis sets (i.e. the coulomb fitting def2/J)<sup>183</sup> when necessary. The hyperfine tensor calculations for the nuclear quadrupole couplings and isotropic hyperfine interactions of pyrrole nitrogen atoms were performed with the B3LYP functional 1777-<sup>179</sup> along with the chain of spheres (RIJCOSX)<sup>184, 185</sup> approximation and an EPR-II<sup>180</sup> and 6-31G(d) basis set for the lighter atoms and magnesium/sulfur, respectively, in the spinunrestricted mode. To account for the influence of solvent effects, a model of uniform dielectric constant of solvents using the conductor-like polarizable continuum model (CPCM) was used in the calculations. <sup>186, 187</sup> The CPCM model used a dielectric constant,  $\varepsilon$ , of 4.0 for incorporating the effects of the protein environment in all of the DFT calculations. All of the calculations included dispersion correction using a DFT-D3 approach with Becke-Johnson damping (D3BJ). Although we employed DFT methods here, note that recent studies by Pantazis and coworkers on highlycoupled Chl a and Pheo molecules in PSII have suggested that refinement of such systems by QM/MM methods is also possible. 188

To assess the computational methods that were employed in previous studies of PSI<sup>88, 89, 189,</sup> and predict the electronic properties of the  $A_0^{\bullet-}$  state of the GsbRC and HbRC, we initially

performed DFT calculations on computational models of  $Chl_{2A}$  and  $Chl_{3A}$  that were derived from the X-ray crystal structure of PSI<sup>2</sup> (PDB ID: 1jb0). As a starting point for the DFT calculations, we selected a simple computational model for  $A_0^{\bullet-}$  that consisted of a monomeric  $Chl\ a^{\bullet-}$  model,  $Chl_{3A}^{\bullet-}$ , and obtained electron spin density distribution across the isolated  $Chl_{3A}^{\bullet-}$  anion that was in agreement with previously published literature on monomeric  $Chl\ a^{\bullet-}$  in vitro. <sup>191-194</sup> Interestingly, while the electron spin density has previously been observed to be uniformly distributed across the pyrrole nitrogen atoms in a  $Chl\ a^{\bullet-}$  cation, <sup>189, 192, 195</sup> we and others have observed that the distribution is asymmetric in a  $Chl\ a^{\bullet-}$  anion. <sup>189, 192</sup> In order to determine the effects of protein-cofactor interactions, we systematically expanded the computational model to include the Met668<sub>PsaA</sub> axial ligand of  $Chl_{3A}$ , a neighboring hydrogen-bonded residue, Tyr696<sub>PsaA</sub>, the A<sub>1A</sub> phylloquinone, the 'accessory' Chl,  $Chl_{2A}$ .

We observed that, with the exception of A<sub>1A</sub>, each additional cofactor that was included in the expanded computational models had a significant impact on the electron density distribution. When compared to the Chl  $a^{\bullet-}$  anion, including the axial ligand, Met668<sub>PsaA</sub>, and hydrogenbonded residue, Tyr696<sub>PsaA</sub> of Chl<sub>3A</sub>•-, we observed a shift in the electron spin density distribution across the pyrrole nitrogens, where three nitrogen atoms had a slight increase in electron density at the expense of the fourth nitrogen. Upon including the 'accessory Chl', Chl<sub>2A</sub>, with its axial water ligand and the A<sub>1A</sub> cofactor or by considering a 'full chain model' with A<sub>1A</sub>, Chl<sub>3A</sub>, Chl<sub>2A/2B</sub>, primary donor Chls, Chl<sub>1A/1B</sub> and their respective ligands, we observed asymmetric delocalization of electron spin density across both Chl<sub>3A</sub> and Chl<sub>2A</sub> in the singly occupied molecular orbital (SOMO) of the  $A_0^{\bullet-}$  state (Figure 7A). Interestingly, the only cofactor that did not demonstrate a discernable impact on charge delocalization in the  $A_0^{\bullet-}$  state was the phylloquinone acceptor,  $A_{1A}$ . The electron spin density distribution in the SOMO of  $A_0^{\bullet-}$ that was observed in the DFT calculations corroborated the delocalization of the unpaired electron spin on at least three nitrogen atoms that was observed in the 2D 14N HYSCORE spectroscopy measurements and yielded a good match between the calculated and experimentally measured hyperfine and quadrupolar coupling constants.<sup>88, 89</sup>

We also compared the electron spin delocalization in the  $A_0^{\bullet-}$  state with that of the  $P_{700}^{\bullet+}$  state of PSI using a computational model that contained  $Chl_{1A}$  and  $Chl_{1B}$  and their respective axial ligands.<sup>2</sup> We observed that the distribution of the electron spin density on the  $Chl_{1A/1B}$  molecules in the SOMO of the primary donor cation,  $P_{700}^{\bullet+190}$ , was similar to the distribution in

the  $A_0^{\bullet-}$  state, albeit to different extents. This indicated that both  $P_{700}^{\bullet+}$  and  $A_0^{\bullet-}$  are comprised of a dimeric chlorophyll motif with extensive electron spin delocalization. Interestingly, while the electron spin density is uniformly distributed across the pyrrole nitrogen atoms on each Chl ring in  $P_{700}^{\bullet+}$ , it was asymmetric in the  $A_0^{\bullet-}$  state, which was similar to earlier observations on Chl  $a^{\bullet+}$  and Chl  $a^{\bullet-}$  in vitro. Moreover, these studies demonstrated that  $A_0$  exists as a dimer of the closely-spaced Chl<sub>2</sub>/Chl<sub>3</sub> molecules wherein the reduced  $A_0^{\bullet-}$  state has an asymmetric distribution of electron spin density that favors Chl<sub>3</sub>. While the electron spin density was also delocalized over the Chl<sub>2</sub>/Chl<sub>3</sub> dimer in the Met688His<sub>PsaA</sub> variant of PSI, there was a small shift in the asymmetry of delocalization in favor of the Chl<sub>2</sub> cofactor. <sup>88,89</sup>

Thus, a combination of experiment and theory led to the first direct determination of electron delocalization over the  $Chl_{2A}$  and  $Chl_{3A}$  dimer in the  $A_0^{\bullet-}$  state of PSI, which was previously thought to be a monomeric Chl electron acceptor. <sup>88, 89</sup> Both the experimental and calculated magnetic parameters and electron spin density distribution in the SOMO was consistent with  $Chl_2/Chl_3$  dimerization in the  $A_0^{\bullet-}$  state of wild-type and Met688His<sub>PsaA</sub> PSI. The uncovering of a dimeric Chl motif in the  $A_0^{\bullet-}$  state has important implications on the development of a new generation of bio-inspired artificial photosynthetic systems. Although experimental data is lacking at this time, we believe that similar DFT calculations of the reduced  $A_0^{\bullet-}$  state of the GsbRC and HbRC will provide important insight on primary charge separation in these RCs. This is because even though both the GsbRC and HbRC contain a homodimeric polypeptide core, there are major differences in the (B)Chl<sub>2</sub> and (B)Chl<sub>3</sub> cofactors of each system. While both BChl<sub>2</sub> and BChl<sub>3</sub> cofactors of the GsbRC are Chl *a* molecules, <sup>4</sup> the recent high-resolution structure of the HbRC has shown that BChl<sub>2</sub> and BChl<sub>3</sub> are BChl g' and 8¹-OH-Chl *a* in the HbRC. <sup>5, 101, 169</sup> Hence, the GsbRC is a homodimeric RC with homodimeric BChl acceptors and the HbRC is a homodimeric RC with heterodimeric BChl/Chl acceptors.

As demonstrated above, DFT is a powerful tool for the investigation of the electronic structure of reduced primary acceptors in RCs. To our best knowledge, quantum-mechanical calculations to determine the electronic structure of the primary acceptors of the homodimeric RCs are lacking at this time. This may be because the high-resolution structures of homodimeric RCs have been determined only very recently. In order to compare the reduced primary acceptor of hetero- and homodimeric Type I RCs, we performed DFT calculations on computational models of  $A_0^{\bullet-}$  in the GsbRC and HbRC from green sulfur bacteria and heliobacteria,

respectively. The goal was to obtain a better understanding of the effect of the relative geometry, symmetry and protein matrix effects on the electronic structure of the dimeric (B)Chl/Chl molecules in the  $A_0^{\bullet-}$  state in of homodimeric RCs.

For the DFT calculations of the homodimeric RCs, the coordinates for the computational models were derived from the structure of the GsbRC and HbRC from Chlorobaculum tepidum (PDB ID: 6m32)<sup>4</sup> and Heliobacterium modesticaldum (PDB ID: 5v8k),<sup>5</sup> respectively. Similar to the computational model of PSI, these models also included the dimeric (B)Chl molecules, BChl<sub>2</sub> and BChl<sub>3</sub> or Chl<sub>3</sub>, the axial ligands to each BChl or Chl monomer and proximal amino acid residues in the binding sites (Figure 3B-C and Table I). The models contained the complete (B)Chl or Chl molecules with the exception that the farnesol or phytol tail was truncated by a methyl group after 4 carbon atoms. Both the GsbRC and HbRC are comprised of a homodimeric polypeptide subunit core encoded by the single genes, pscA and pshA, respectively. However, the similarity is broken by the presence of a Chl a dimer in the GsbRC and a BChl  $g^{2}/8^{1}$ -OH-Chl a dimer in the HbRC. The DFT calculations were performed with B3LYP level of theory using an EPR-II and 6-31G(d) basis set for the lighter atoms and Mg and S, respectively. The electron spin density distribution in the SOMO of  $A_0^{\bullet-}$  obtained from the DFT calculations indicated that while the unpaired electron spin is symmetrically distributed across the Chl<sub>2</sub>/Chl<sub>3</sub> dimer of Chl a molecules in the GsbRC, it is completely asymmetric and solely localized on Chl<sub>3</sub> (the 8<sup>1</sup>-OH-Chl a) cofactor in the  $A_0^{\bullet}$  state of the HbRC (Figure 7B-C). This was also reflected in the calculated isotropic hyperfine coupling constants, A<sub>iso</sub>, of A<sub>0</sub><sup>•</sup> in the GsbRC and HbRC. The A<sub>iso</sub> couplings of the nitrogen atoms of the Chl<sub>2</sub>/Chl<sub>3</sub> dimer in the A<sub>0</sub><sup>•-</sup> state of the GsbRC were typically smaller and similar in magnitude to those of the  $A_0^{\bullet-}$  and  $P_{700}^{\bullet+}$  state of PSI. <sup>88, 89</sup> In contrast, the  $A_{iso}$  couplings of the nitrogen atoms in  $A_0^{\bullet-}$  of the HbRC were larger in magnitude and mirrored the couplings of monomeric Chl  $a^{\bullet-}$  and Chl  $a^{\bullet+}$  in vitro.

#### **Design principles of Type I Reaction Centers**

There are several common design principles found in each  $A_0$  pair in Type I RCs. Perhaps the most apparent is the architecture of the (B)Chl molecules themselves. With only minor deviations in terms of Mg – Mg distance, they all attain a parallel orientation of their ring structures, resulting in significant  $\pi$ -stacking. Further, the overlapping region of these Chls are identical in all Type I RCs, with ring II and ring III of (B)Chl<sub>2</sub> overlapping with ring II and ring

III of Chl<sub>3</sub>, respectively. When we extend this consideration outward to the interacting protein matrix, one common thread among all  $A_0$  dimers lies in the relative strength of the axial ligands. It is well known that certain ligands have a more significant impact on the redox potential of Chls than others, with a general trend of more negative to more positive potentials being His > Ser > Water > Met.<sup>13</sup> With that in mind, for the axial ligands associated with (B)Chl<sub>2</sub> and Chl<sub>3</sub>, ligands to Chl<sub>3</sub> never have a more negative impact on redox potential than the ligand of Chl<sub>2</sub>. In PS I this manifests as  $H_2O$  for Chl<sub>2</sub> (-1.87 V at  $\varepsilon = 4$ ) and Met for Chl<sub>3</sub> (-1.79 V at  $\varepsilon = 4$ ). Indeed, only in the HbRC do these forces begin to equalize, as each cofactor is ligated by a water molecule. But even then, at  $\varepsilon = 4$  a water molecule will drive a BChl more slightly more negative than a Chl (-1.89 V and -1.87 V, respectively). This common trend is likely in place to help drive forward electron transfer by making Chl<sub>3</sub> more oxidizing than Chl<sub>2</sub>.

Recently, there have been exciting developments that have allowed for mutations to be made within the HbRC, with some of the first being to the A<sub>0</sub> binding pocket. Namely, two of the residues that coordinate the 8¹-OH Chl a: Ser553<sub>PshA</sub> and Ser545<sub>PshA</sub>. <sup>196</sup> Ser545<sub>PshA</sub> supports the water molecules that serve as the axial ligand, while Ser553<sub>PshA</sub> provides a hydrogen bond.<sup>5</sup> Changing Ser $545_{PshA}$  to Met caused the most drastic changes, where no  $8^1$ -OH Chl a was found in the RC and no charge separation was detected. This suggests larger scale structural changes, potentially involving the water pocket near Chl<sub>3</sub>. Removal of the hydrogen bond by replacing the Ser residue by Ala resulted in an expected negative shift of the redox potential, accelerating both forward electron transfer and charge recombination by  $\sim 50$  ps and  $\sim 15$  ns, respectively. Similar results were also observed when the axial ligand was changed to His. This is not surprising as a His ligand is expected to drive the redox potential more negative than a water ligand. <sup>13</sup> Along with the change to electron transfer rates, the quantum efficiency of charge separation  $(\Phi)$  for the Ala and His variants changed from 1.0 to 0.822 and 0.717, respectively. 196 Analogous effects were seen in PSI with the Met axial ligand to Chl<sub>3A</sub> was replaced by a His residue. In the subset of RCs where the His ligated Chl<sub>3A</sub>, forward electron transfer was inhibited because of the impact to the redox potential.  $^{96}$  This data suggests that the  $A_0$  binding pockets are optimized on an energetic knife edge, specifically tuned to maximize both charge separation and forward electron transfer reactions while also inhibiting charge recombination.

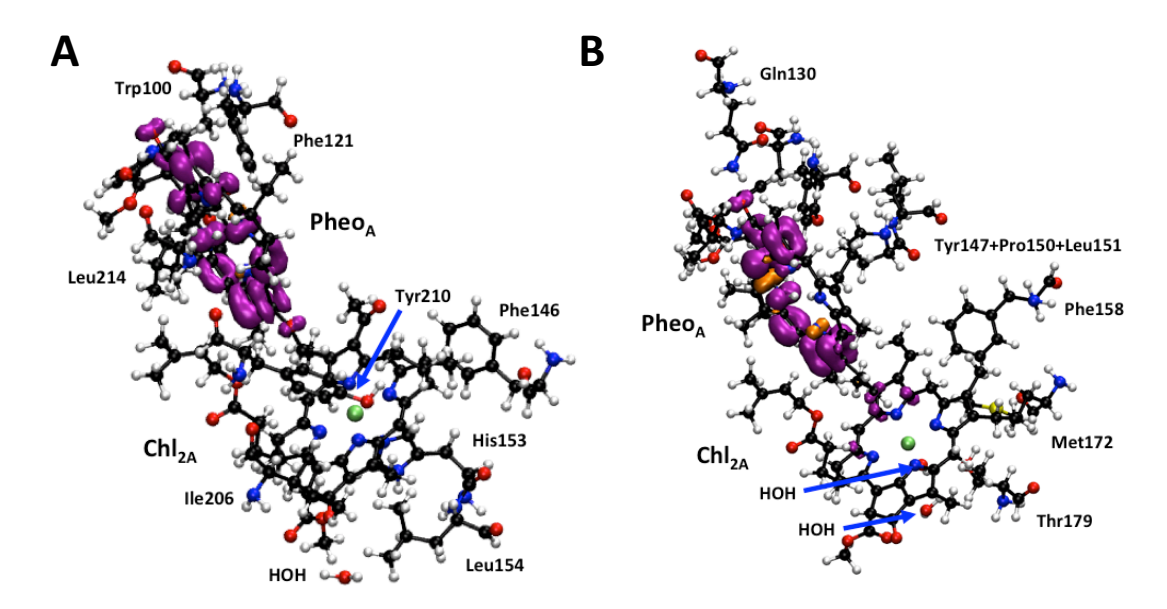


**Figure 8.** Comparison of the electronic structure of the  $A_0^-$  state of (A) the bRC from *Rba. sphaeroides* and (B) PSII based on the electron spin density distribution in the SOMO obtained by DFT methods.

It appears these different factors have a profound influence on the distribution of electron density across both pairs of Chls. Perhaps the strongest factor that influences this distribution is the identity of the cofactors themselves. As seen in the HbRC, where  $A_0$  is a heterodimer composed of chemically distinct (B)Chls leading to a significant asymmetry in electron spin delocalization that highly favors Chl<sub>3</sub>. While the geometric properties mirror other Type I RCs, the electronic properties of the primary acceptor system of the HbRC more closely resembles that of Type II RCs (see below). This factor in asymmetry is not present in PSI and the GsbRC as they are composed of dimer of identical Chls. In these Chl systems, asymmetry is controlled by axial ligands and the surrounding protein matrix. For PSI, the Met688 and H-bonded Tyr696<sub>A</sub> slightly shifts electron distribution in favor of Chl<sub>3</sub> by a factor of 3. While  $A_0$  for the GsbRC does have minor differences in how the protein matrix interacts with each Chl, the axial ligand to each Chl is identical. This results in an  $A_0$  acceptor closest to that of a true homodimer, where electron density is shared nearly equally across both rings. The impact of this delocalization on electron transfer is not fully understood; though, as seen in PSI when the axial ligand to Chl<sub>3A</sub> was changed<sup>89</sup>, it likely helps to ensure forward electron transfer is efficient.

## Electronic Structure of A<sub>0</sub> in Type II Reaction Centers

In order to compare the electronic structure of the  $A_0^{\bullet-}$  state across both Type I and Type II RCs, we also performed DFT calculations of the  $A_0^{\bullet-}$  state of the bRC from Rba. sphaeroides and PSII. The coordinates of the computational models were derived from the X-ray crystal structure of the bRC from Rba. sphaeroides (PDB ID: 1pcr)<sup>197</sup> and PSII (PDB ID: 3wu2).<sup>3</sup> Each model included the (B)Chl<sub>2A</sub>/(B)Pheo<sub>A</sub> molecules, the axial ligand of (B)Chl<sub>2A</sub> and proximal hydrogen-bonding and hydrophobic residues in the protein matrix as observed in the respective structures (Figures 5A-B and Table II). The DFT methods employed were as described in the previous section. The computational models contained the complete (B)Chl<sub>A</sub> and (B)Pheo<sub>A</sub> molecules with the phytol tail truncated with a methyl group after four carbon atoms. To determine the effects of protein-cofactor interactions, we included the axial ligand of each (B)Chl<sub>A</sub> molecule, the putative hydrogen bonding and hydrophobic/aromatic residues in the vicinity of the (B)Chl and (B)Pheo molecules (Table II). We observed an asymmetric distribution of the electron spin density in the singly occupied molecular orbital (SOMO) of the  $A_0^{\bullet-}$  state in both the bRC and PSII, where the electron was predominantly localized on the (B)PheoA molecule. This was in agreement with the hyperfine coupling constants that were observed in previous ENDOR, ESEEM and HYSCORE spectroscopy studies 70, 71, 198 and previous DFT calculations on the bRC and a homology model of PSII. 199, 200 The localization of electron spin density on the (B)Pheo<sub>A</sub> molecule in the SOMO is consistent with the relative geometry of the (B)Chl<sub>A</sub> and (B)Pheo<sub>A</sub> molecules in the bRC and PSII. As shown in Figure 6, the ring planes of (B)Chl<sub>A</sub> and (B)Pheo<sub>A</sub> are not oriented parallel to each, in stark contrast to A<sub>0</sub> of Type I RCs (Figure 4); instead, their ring planes are in a nearly perpendicular orientation. This results in virtually no overlap of their macrocycles. However, the localization of the electron on the (B)PheoA of the bRC and PSII is in contrast with the extensive electron spin delocalization that was observed in PSI and the GsbRC.

#### **Common design principles of Type II Reaction Centers**

Type II RCs have remarkably consistent features in their primary acceptor sites. Perhaps the most obvious feature is the distances and orientation of their (B)Chl<sub>2</sub>/Pheo pair. While Type I RCs have small but non-trivial changes in the distance between their cofactors that vary in different organisms, Type II RCs remain virtually identical, even in significantly divergent species. Further, there is no deviation in the chemical identity of the (B)Chls and Pheos used in the early donor-acceptor system. Whereas in Type I RCs, the identity of (B)Chl<sub>3</sub> has been

observed to differ from the remaining four (B)Chls,<sup>5</sup> and in Gsb the primary donor identity is different from that of  $A_0$ ,<sup>4</sup> Type II RCs are always consistent with the (B)Chl/Pheo identity. The importance of this fact becomes clear when the BPheo molecule is replaced with Pheo in the bRC. The change in redox potential of  $\sim 200 \text{ mV}^{201, 202}$  results in forward electron transfer being blocked from BChl<sub>2</sub>.<sup>203</sup> Further, the Pheo from each RC are lined with a series of aromatic residues, that likely help with the binding of the cofactor. Most notably are two residues interacting with quadrant III of the macrocycle, adopting a similar orientation with respect to the ring plane. Similarly, opposite to those is a Leu residue in nearly identical positions in each RC.

It has been suggested that the drop in free energy associated with electron transfer from a (B)Chl<sub>2A</sub> to (B)Pheo<sub>A</sub> is the sole driving force for these early electron transfer steps. <sup>85</sup> While it may be a major component, the surrounding protein matrix has a significant effect. For instance, the Tyr210<sub>M</sub> associated with BChl<sub>2A</sub> has been replaced by a Phe and Leu, both of which are common features of (B)Chl binding sites. Each modification had a significant impact on BChl<sub>2</sub>, resulting in slowed electron transfer rates and allowing the intermediate, BChl<sub>2A</sub>•-, to be resolved. <sup>204</sup>

## Comparison of Primary Acceptors of Type I and Type II Reaction Centers

It is apparent that Type I and Type II RCs employ superficially similar, yet significantly different motifs of the primary donor and acceptor that are involved in charge separation. Indeed, even within each archetype there are subtle differences leading to interesting functional changes. For example, the Type II RCs, bRC and PSII, both have monomeric  $A_0$  acceptors with high structural similarity; the electron spin density is localized on (B)Pheo<sub>A</sub> in the reduced  $A_0^{\bullet}$  state. In contrast, Type I RCs contain a highly conserved overlapping motif of (B)Chl<sub>2</sub> and (B)Chl<sub>3</sub> molecules in the  $A_0$  cofactor, but the extent of delocalization of the electron spin density across the two (B)Chl rings in the reduced  $A_0^{\bullet}$  state varies significantly across RCs from different organisms. Moreover, in comparison with the homodimeric GsbRC and HbRC, the heterodimeric PSI RC displays a preference for electron transfer along the A-branch of cofactors that is largely determined by the six Chl molecules housed within the core polypeptides. <sup>50, 53</sup>

The evolutionary drive from a homodimeric RC, where both branches remain active and in equal use, toward a skewed bidirectional or solely unidirectional electron transfer pathway observed in most heterodimeric RCs remains unstudied. The inactivation of one of the electron

transfer pathways may appear to be the result of a loss of evolutionary fitness, however, it does not appear to be the case. The heterodimerization of RC core may be a means of specializing RC branches. In Type II RCs, this manifests as a means to extend the charge separated state,  $P^{\bullet^+}Q_B^{\bullet}$ . Upon the first reduction of  $Q_B$  to  $Q_B^{\bullet^-}$ , the RC must be allowed another turnover before the mobile  $Q_BH_2$  can form. Not only does this mean re-reduction of  $P^{\bullet^+}$ , but also competing with the slower process of adding a proton and second electron to  $Q_B^{\bullet^-}$ . Deactivation of the branch associated with  $Q_B$  makes the primary donor functionally 'farther' from  $Q_B$ , increasing the lifetime before charge recombination and allowing another turnover of the RC<sup>100</sup>. Specialization of RC branches in this way provides such a powerful evolutionary advantage that the process occurred separately in the ancestors of PSII and the bRC.<sup>26, 206</sup> These advantages are not exclusive to Type II RCs. In PSI, heterodimerization appears to have arisen from the necessity to prevent the formation of the reactive oxygen species singlet oxygen ( $^1O_2$ ) and superoxide ( $O_2^-$ ) caused by recombination from  $A_0$  and a long-lived  $F_X^{\bullet^-}$  state, respectively.<sup>207</sup> Such specialization is not necessary in the homodimeric Type I RCs, as these species live in anoxic environments.

The question arises as to why two different primary acceptor motifs arose in Type I and Type II RCs. After all, neither appears to be more or less efficient either in generating the initial charge separated state or encouraging forward electron transfer. Type II RCs gain the advantage of a guaranteed drop in free energy by using (B)Pheo as the primary acceptor, limiting the need for extensive protein-cofactor interactions. Further, the similar identity of the (B)Chls/(B)Pheos doesn't require large scale changes to the (B)Chl biosynthetic pathway. While Type II RCs appear to benefit from the fixed nature of their acceptors, the primary benefit afforded to Type I RCs is flexibility. There appears to be significant latitude in determining which flavors of (B)Chl can be used that still allows the charge-separation and efficient electron transfer. Expanding the spectral region of light absorption, even slightly, by incorporating different (B)Chls may provide a survival advantage. Moreover, Type I RCs have a much more diverse set of electron-transfer cofactors than Type IIs. PSI can be thought of as containing the full complement of cofactors, including a phylloquinone and bound ferredoxin. The GsbRC lacks a quinone, yet retains the bound ferredoxin, albeit loosely. In the extreme case of the HbRC, it lacks all of those features. Moreover, the distances between F<sub>X</sub> and the preceding cofactors vary among the three RCs, from  $\sim$  12 Å in PS I to  $\sim$  15 Å in GsbRC. As such, the acceptor system in Type I RCs must have been energetically adaptable to field such an array of electron transfer conditions. Employing a dimeric motif provides an opportunity to control the extent of dimerization and delocalization, and thus the energetics of the cofactor, making such changes less difficult to overcome. Unfortunately, without having detailed information on ancestral versions of Type I and Type II RCs, it is difficult to explain such differences. While this area of research is highly contested, a prevailing model suggests that Type I and Type II RCs likely share a common homodimeric ancestral RC with shared properties. <sup>26, 208</sup> The nature of this ancestral RC remains elusive, and we do not know if the original donor-acceptor system was monomeric, dimeric, or something else entirely.

In looking forward to important applications, the principles that have been discussed here stand out. Perhaps one of the most underappreciated aspects of photosynthetic RCs is their unique ability to use identical cofactors for multiple purposes. As seen here, (B)Chl molecules can be employed both as electron donors and acceptors, in addition to light harvesting machinery. This is owed in large part to the energetic or redox flexibility of (B)Chl molecules. Variations in the axial ligands are well known methods of altering reduction potentials of (B)Chls. 13 Additionally, the presence of charged or non-polar species, as well as H-bonds are effective methods of shift the relative redox potentials neighboring (B)Chls to enable efficient and stable electron transfer processes. Moreover, as seen here, (B)Chls allow for an additional tuning effect in the form of cofactor dimerization. <sup>22, 88, 89</sup> (B)Chls have the ability to form dimers, or even multimers, 51, 53, 55, 209 with strength of their coupling, and thus the change in potential of the dimer itself, being adjusted by the distance between monomers, their relative orientation, and the aforementioned protein-matrix interactions to each monomer. Employing similarly robust and tunable ensembles of cofactors could provide an opportunity for a surrounding immobilizing matrix to adjust the redox potential of individual molecules as well as the multimeric systems they compose. In doing so, stable and efficient electron transfer reactions could be allowed.

One additional note must be made here regarding the use of chemically similar molecules as seen in the (B)Pheos of Type II RCs and different (B)Chls that compose the A<sub>0</sub> system of the HbRC. Both instances showcase the advantage of using molecules with energetic or redox flexibility, as relatively small changes to the molecules themselves allow for consistent and controllable changes. The loss of a central Mg<sup>2+</sup> resulting in the formation of the (B)Pheo is a relatively straight forward way to direct electron transfer<sup>85</sup>. While such a method is useful in many cases, it loses flexibility that may be necessary in a more complicated matrix of acceptors.

In the latter case of the HbRC, clearly it is possible to allow electron transfer, and even dimerization, using two dissimilar (B)Chls molecules. This method could be employed to provide some measure of gated electron transfer, where an acceptor,  $A_1$ , is energetically uphill from the donor, D, and successful electron transfer is only allowed via the redox state of subsequent acceptor(s),  $A_2...A_n$ . Adjusting the energetic 'height' of this gate by increasing or lowering the relative potentials of  $A_1$  or  $A_n$  could be a useful means of controlling electron flow. Such a system would hold even for a dimeric acceptor of  $A_1$ - $A_1$ ', where  $A_1$ ' is energetically uphill relative to  $A_1$ .

An additional consequence of this system is that electron transfer is, in theory, controllable and perhaps even tunable under a variety of conditions. Photosynthetic RCs are largely designed to vector an electron is a single direction. In homodimeric Type I RCs, this means utilization of both branches, and in Type II RCs it translates to specialization of one branch at the expense of the other. But as we have discussed here, PSI is a rather unique case whereby electron transfer is favors one branch, but not exclusively. This provides a proof of concept for branching electron transfer, where the degree of branch specificity is controlled within a matrix of chemically identical molecules. While biological necessity dictates that both branches terminate at the same point, it may be possible to generate a fully branching electron transfer pathway terminating in different locations that serve differing functions. The degree of branch utilization could, in turn, be controlled by the nature of the immobilizing matrix as has been proposed in PSI. Further, in much the same way that electron transfer rates from various cofactors in PSI are influenced by external pressures like temperature <sup>32, 211, 212</sup> or chemical additives, <sup>34, 213, 214</sup> it may be possible to create an artificial photosynthetic system that adapts to the surrounding environment.

## Acknowledgments

This study is supported by the Photosynthetic Systems Program, Office of Basic Energy Sciences of the U.S. Department of Energy under the contracts DE-FG02-07ER15903 (KVL) and DE-FG-05-05-ER46222 (JHG). The authors acknowledge support from the NSF Graduate Research Fellowship Program (GRFP) for PL, NSF Research Experience for Undergraduates (REU) Program (grant number 1560266) for EG and AM, New Faculty Start-up Funds from Brock University for DK and the Center for Computational Innovations (CCI) at RPI and the Natural Sciences and Engineering Research Council of Canada (NSERC) for computational resources.

## References

- [1] Stowell, M. H. B., McPhillips, T. M., Rees, D. C., Soltis, S. M., Abresch, E., and Feher, G. (1997) Light-induced structural changes in photosynthetic reaction center: Implications for mechanism of electron-proton transfer, *Science* 276, 812–816.
- [2] Jordan, P., Fromme, P., Witt, H. T., Klukas, O., Saenger, W., and Krauss, N. (2001) Three-dimensional structure of cyanobacterial photosystem I at 2.5 A resolution, *Nature 411*, 909–917.
- [3] Umena, Y., Kawakami, K., Shen, J. R., and Kamiya, N. (2011) Crystal structure of oxygenevolving photosystem II at a resolution of 1.9 Å, *Nature 473*, 55–60.
- [4] Chen, J.-H., Wu, H., Xu, C., Liu, X.-C., Huang, Z., Chang, S., Wang, W., Han, G., Kuang, T., Shen, J.-R., and Zhang, X. (2020) Architecture of the photosynthetic complex from a green sulfur bacterium, *Science* 370, eabb6350.
- [5] Gisriel, C., Sarrou, I., Ferlez, B., Golbeck, J. H., Redding, K. E., and Fromme, R. (2017) Structure of a symmetric photosynthetic reaction center-photosystem, *Science* 357, 1021–1025.
- [6] Tice, M. M., and Lowe, D. R. (2004) Photosynthetic microbial mats in the 3,416-Myr-old ocean, *Nature 431*, 549–552.
- [7] Şener, M., Strümpfer, J., Hsin, J., Chandler, D., Scheuring, S., Hunter, C. N., and Schulten, K. (2011) Förster energy transfer theory as reflected in the structures of photosynthetic light-harvesting systems, *Chem Phys Chem 12*, 518–531.
- [8] Hogewoning, S. W., Wientjes, E., Douwstra, P., Trouwborst, G., van Ieperen, W., Croce, R., and Harbinson, J. (2012) Photosynthetic quantum yield dynamics: From photosystems to leaves *Plant Cell* 24, 1921–1935.
- [9] Tomi, T., Shibata, Y., Ikeda, Y., Taniguchi, S., Haik, C., Mataga, N., Shimada, K., and Itoh, S. (2007) Energy and electron transfer in the photosynthetic reaction center complex of *Acidiphilium rubrum* containing Zn-bacteriochlorophyll *a* studied by femtosecond upconversion spectroscopy, *Biochim Biophys Acta 1767*, 22–30.
- [10] He, Z., Ferlez, B., Kurashov, V., Tank, M., Golbeck, J. H., and Bryant, D. A. (2019) Reaction centers of the thermophilic microaerophile, *Chloracidobacterium thermophilum*

- (Acidobacteria) I: Biochemical and biophysical characterization, *Photosynth Res 142*, 87–103.
- [11] Charles, P., Kalendra, V., He, Z., Khatami, M. H., Golbeck, J. H., van der Est, A., Lakshmi, K. V., and Bryant, D. A. (2020) Two-dimensional <sup>67</sup>Zn HYSCORE spectroscopy reveals that a Zn-bacteriochlorophyll a<sub>P</sub>' dimer is the primary donor (P<sub>840</sub>) in the type-1 reaction centers of *Chloracidobacterium thermophilum*, *Phys Chem Chem Phys* 22, 6457–6467.
- [12] Björn, L. O., Papageorgiou, G. C., Blankenship, R. E., and Govindjee. (2009) A viewpoint: Why chlorophyll *a*?, *Photosyn Res 99*, 85–98.
- [13] Heimdal, J., Jensen, K. P., Devarajan, A., and Ryde, U. (2007) The role of axial ligands for the structure and function of chlorophylls, *J Biol Inorg Chem 12*, 49–61.
- [14] Oren, A. (2011) Characterization of pigments of prokaryotes and their use in taxonomy and classification, In *Methods in Microbiology* (Rainey, F., and Oren, A., Eds.), pp 261–282, Academic Press.
- [15] Steglich, C., Mullineaux, C. W., Teuchner, K., Hess, W. R., and Lokstein, H. (2003) Photophysical properties of *Prochlorococcus marinus* SS120 divinyl chlorophylls and phycoerythrin *in vitro* and *in vivo*, *FEBS Lett* 553, 79–84.
- [16] Ito, H., and Tanaka, A. (2011) Evolution of a divinyl chlorophyll-based photosystem in *Prochlorococcus*, *Proc Natl Acad Sci USA 108*, 18014–18019.
- [17] Barrera-Rojas, J., de la Vara, L. G., Ríos-Castro, E., Leyva-Castillo, L. E., and Gómez-Lojero, C. (2018) The distribution of divinyl chlorophylls *a* and *b* and the presence of ferredoxin-NADP<sup>+</sup> reductase in *Prochlorococcus marinus* MIT9313 thylakoid membranes, *Heliyon 4*, e01100.
- [18] Moore, L. R., Goericke, R., and Chisholm, S. W. (1995) Comparative physiology of *Synechococcus* and *Prochlorococcus*: Influence of light and temperature on growth, pigments, fluorescence and absorptive properties, *Mar Ecol Prog Ser 116*, 259–275.
- [19] Partensky, F., Hess, W. R., and Vaulot, D. (1999) *Prochlorococcus*, a marine photosynthetic prokaryote of global significance, *Microbiol Mol Biol Rev 63*, 106–127.
- [20] Chew, A. G. M., and Bryant, D. A. (2007) Chlorophyll biosynthesis in bacteria: The origins of structural and functional diversity, *Annu Rev Microbiol* 61, 113–129.
- [21] Ralf, G., and Repeta, D. J. (1992) The pigments of *Prochlorococcus marinus*: The presence of divinylchlorophyll *a* and *b* in a marine procaryote, *Limnol Oceanogr* 37, 425–433.

- [22] Gorka, M., Baldansuren, A., Malnati, A., Gruszecki, E., Golbeck, J. H., and Lakshmi, K. V. (2021) Shedding light on primary donors in photosynthetic reaction centers, *Front Microbiol* 12.
- [23] Hager-Braun, C., Zimmermann, R., and Hauska, G. (1999) The homodimeric reaction center of *Chlorobium*, In *The Phototrophic Prokaryotes* (Peschek, G. A., Löffelhardt, W., and Schmetterer, G., Eds.), pp 169–181, Springer US, Boston, MA.
- [24] Hauska, G., Schoedl, T., Remigy, H., and Tsiotis, G. (2001) The reaction center of green sulfur bacteria, *Biochim Biophys Acta* 1507, 260–277.
- [25] Yamada, M., Zhang, H., Hanada, S., Nagashima, K. V. P., Shimada, K., and Matsuura, K. (2005) Structural and spectroscopic properties of a reaction center complex from the chlorosome-lacking filamentous anoxygenic phototrophic bacterium *Roseiflexus castenholzii*, *J Bacteriol* 187, 1702–1709.
- [26] Cardona, T. (2015) A fresh look at the evolution and diversification of photochemical reaction centers, *Photosynth Res* 126, 111–134.
- [27] Mimuro, M., Tomo, T., Nishimura, Y., Yamazaki, I., and Satoh, K. (1995) Identification of a photochemically inactive pheophytin molecule in the spinach D<sub>1</sub>-D<sub>2</sub>-Cyt b<sub>559</sub> complex, *Biochim Biophys Acta Bioenerg* 1232, 81–88.
- [28] Wakeham, M. C., and Jones, M. R. (2005) Rewiring photosynthesis: Engineering wrongway electron transfer in the purple bacterial reaction centre, *Biochem Soc Trans* 33, 851-857.
- [29] Williams, J. C., and Allen, J. P. (2009) Directed modification of reaction centers from purple bacteria, In *The Purple Phototrophic Bacteria* (Hunter, C. N., Daldal, F., Thurnauer, M. C., and Beatty, J. T., Eds.), pp 337–353, Springer Netherlands, Dordrecht.
- [30] Vinyard, D. J., Ananyev, G. M., and Dismukes, C. (2013) Photosystem II: The reaction center of oxygenic photosynthesis, *Annu Rev Biochem* 82, 577–606.
- [31] Golbeck, J. H. (2006) *Photosystem I: The Light-Driven Plastocyanin: Ferredoxin Oxidoreductase*, Springer, Dordrecht.
- [32] Agalarov, R., and Brettel, K. (2003) Temperature dependence of biphasic forward electron transfer from the phylloquinone(s) A<sub>1</sub> in photosystem I: Only the slower phase is activated, *Biochim Biophys Acta 1604*, 7–12.

- [33] Poluektov, O. G., Paschenko, S. V., Utschig, L. M., Lakshmi, K. V., and Thurnauer, M. C. (2005) Bidirectional electron transfer in photosystem I: Direct evidence from high-frequency time-resolved EPR spectroscopy, *J Am Chem Soc* 127, 11910–11911.
- [34] Kurashov, V., Gorka, M., Milanovsky, G. E., Johnson, T. W., Cherepanov, D. A., Semenov, A. Y., and Golbeck, J. H. (2018) Critical evaluation of electron transfer kinetics in P<sub>700</sub>-F<sub>A</sub>/F<sub>B</sub>, P<sub>700</sub>-F<sub>X</sub>, and P<sub>700</sub>-A<sub>1</sub> photosystem I core complexes in liquid and in trehalose glass, *Biochim Biophys Acta Bioenerg* 1859, 1288–1301.
- [35] Srinivasan, N., Chatterjee, R., Milikisiyants, S., Golbeck, J. H., and Lakshmi, K. V. (2011) Effect of hydrogen bond strength on the redox properties of phylloquinones: A two-dimensional hyperfine sublevel correlation spectroscopy study of photosystem I, *Biochemistry* 50, 3495–3501.
- [36] Srinivasan, N., and Golbeck, J. H. (2009) Protein-cofactor interactions in bioenergetic complexes: The role of the A<sub>1A</sub> and A<sub>1B</sub> phylloquinones in photosystem I, *Biochim Biophys Acta 1787*, 1057–1088.
- [37] Shen, G., Antonkine, M. L., van der Est, A., Vassiliev, I. R., Brettel, K., Bittl, R., Zech, S. G., Zhao, J., Stehlik, D., Bryant, D. A., and Golbeck, J. H. (2002) Assembly of photosystem I: II. Rubredoxin is required for the *in vivo* assembly of F<sub>X</sub> in *Synechococcus* sp. PCC 7002 as shown by optical and EPR spectroscopy, *J Biol Chem* 277, 20355–20366.
- [38] Wraight, C. (2004) Proton and electron transfer in the acceptor quinone complex of photosynthetic reaction centers from *Rhodobacter sphaeroides*, *Front Biosci* 9, 309–337.
- [39] White, N. T. H., Beddard, G. S., Thorne, J. R. G., Feehan, T. M., Keyes, T. E., and Heathcote, P. (1996) Primary charge separation and energy transfer in the photosystem I reaction center of higher plants, *J Phys Chem 100*, 12086–12099.
- [40] Savikhin, S., Xu, W., Chitnis, P. R., and Struve, W. S. (2000) Ultrafast primary processes in PS I from *Synechocystis* sp. PCC 6803: Roles of P<sub>700</sub> and A<sub>0</sub>, *Biophys J* 79, 1573–1586.
- [41] Gibasiewicz, K., Ramesh, V. M., Melkozernov, A. N., Lin, S., Woodbury, N. W., Blankenship, R. E., and Webber, A. N. (2001) Excitation dynamics in the core antenna of PS I from *Chlamydomonas reinhardtii* CC 2696 at room temperature, *J Phys Chem B 105*, 11498–11506.
- [42] Gobets, B., and van Grondelle, R. (2001) Energy transfer and trapping in photosystem I, *Biochim Biophys Acta Bioenerg* 1507, 80–99.

- [43] Gobets, B., van Stokkum, I. H., Rögner, M., Kruip, J., Schlodder, E., Karapetyan, N. V., Dekker, J. P., and van Grondelle, R. (2001) Time-resolved fluorescence emission measurements of photosystem I particles of various cyanobacteria: a unified compartmental model, *Biophys J* 81, 407–424.
- [44] Melkozernov, A. N. (2001) Excitation energy transfer in Photosystem I from oxygenic organisms, *Photosynth Res* 70, 129–153.
- [45] Savikhin, S., and Jankowiak, R. (2014) Mechanism of primary charge separation in photosynthetic reaction centers, In *The Biophysics of Photosynthesis* (Golbeck, J. H., and van der Est, A., Eds.), pp 193–240, Springer, New York, NY.
- [46] van Brederode, M. E., Jones, M. R., van Mourik, F., van Stokkum, I. H. M., and van Grondelle, R. (1997) A new pathway for transmembrane electron transfer in photosynthetic reaction centers of *Rhodobacter sphaeroides* not involving the excited special pair, *Biochemistry* 36, 6855–6861.
- [47] van Brederode, M. E., Ridge, J. P., van Stokkum, I. H. M., van Mourik, F., Jones, M. R., and van Grondelle, R. (1998) On the efficiency of energy transfer and the different pathways of electron transfer in mutant reaction centers of *Rhodobacter sphaeroides*, *Photosynth Res* 55, 141–146.
- [48] Holzwarth, A. R., Müller, M. G., Niklas, J., and Lubitz, W. (2006) Ultrafast transient absorption studies on photosystem I reaction centers from *Chlamydomonas reinhardtii*. 2: Mutations near the P<sub>700</sub> reaction center chlorophylls provide new insight into the nature of the primary electron donor, *Biophys J 90*, 552–565.
- [49] Müller, M. G., Niklas, J., Lubitz, W., and Holzwarth, A. R. (2003) Ultrafast transient absorption studies on photosystem I reaction centers from *Chlamydomonas reinhardtii*. 1. A new interpretation of the energy trapping and early electron transfer steps in photosystem I, *Biophys J* 85, 3899–3922.
- [50] Müller, M. G., Slavov, C., Luthra, R., Redding, K. E., and Holzwarth, A. R. (2010) Independent initiation of primary electron transfer in the two branches of the photosystem I reaction center, *Proc Natl Acad Sci U S A 107*, 4123–4128.
- [51] Cherepanov, D. A., Shelaev, I. V., Gostev, F. E., Aybush, A. V., Mamedov, M. D., Shuvalov, V. A., Semenov, A. Y., and Nadtochenko, V. A. (2020) Generation of ion-

- radical chlorophyll states in the light-harvesting antenna and the reaction center of cyanobacterial photosystem I, *Photosynth Res* 146, 55-73.
- [52] Cherepanov, D. A., Shelaev, I. V., Gostev, F. E., Mamedov, M. D., Petrova, A. A., Aybush, A. V., Shuvalov, V. A., Semenov, A. Y., and Nadtochenko, V. A. (2017) Mechanism of adiabatic primary electron transfer in photosystem I: femtosecond spectroscopy upon excitation of reaction center in the far-red edge of the Q<sub>Y</sub> band, *Biochim Biophys Acta Bioenerg* 1858, 895–905.
- [53] Cherepanov, D. A., Shelaev, I. V., Gostev, F. E., Petrova, A., Aybush, A. V., Nadtochenko, V. A., Xu, W., Golbeck, J. H., and Semenov, A. Y. (2021) Primary charge separation within the structurally symmetric tetrameric Chl<sub>2A</sub>P<sub>A</sub>P<sub>B</sub>Chl<sub>2B</sub> chlorophyll exciplex in photosystem I, J Photochem Photobiol B 217, 112154.
- [54] Kojima, R., Yamamoto, H., Azai, C., Uragami, C., Hashimoto, H., Kosumi, D., and Oh-oka, H. (2020) Energy transfer and primary charge separation upon selective femtosecond excitation at 810 nm in the reaction center complex from *Heliobacterium modesticaldum*, *J Photochem Photobiol A 401*, 112758.
- [55] Song, Y., Sechrist, R., Nguyen, H. H., Johnson, W., Abramavicius, D., Redding, K. E., and Ogilvie, J. P. (2021) Excitonic structure and charge separation in the heliobacterial reaction center probed by multispectral multidimensional spectroscopy, *Nature Commun* 12, 2801.
- [56] Vos, M. H., Breton, J., and Martin, J.-L. (1997) Electronic energy transfer within the hexamer cofactor system of bacterial reaction centers, *J Phys Chem B* 101, 9820–9832.
- [57] Shuvalov, V. A., and Klimov, V. V. (1976) The primary photoreactions in the complex cytochrome-P-890 · P-760 (bacteriopheophytin<sub>760</sub>) of *Chromatium minutissimum* at low redox potentials, *Biochim Biophys Acta*, *Bioenerg 440*, 587–599.
- [58] Tiede, D. M., Prince, R. C., and Dutton, P. L. (1976) EPR and optical spectroscopic properites of the electron carrier intermediate between the reaction center bacteriochlorophylls and the primary acceptor in *Chromatium vinosum*, *Biochim Biophys Acta*, *Bioenerg 449*, 447–467.
- [59] Okamura, M. Y., Isaacson, R. A., and Feher, G. (1979) Spectroscopic and kinetic properties of the transient intermediate acceptor in reaction centers of *Rhodopseudomonas* sphaeroides, *Biochim Biophys Acta, Bioenerg* 546, 394–417.

- [60] Deisenhofer, J., Epp, O., Miki, K., Huber, R., and Michel, H. (1985) Structure of the protein subunits in the photosynthetic reaction centre of *Rhodopseudomonas viridis* at 3 Å resolution, *Nature 318*, 618–624.
- [61] Arlt, T., Schmidt, S., Kaiser, W., Lauterwasser, C., Meyer, M., Scheer, H., and Zinth, W. (1993) The accessory bacteriochlorophyll: A real electron carrier in primary photosynthesis, *Proc Natl Acad Sci U S A 90*, 11757–11761.
- [62] van Stokkum, I. H. M., Beekman, L. M. P., Jones, M. R., van Brederode, M. E., and van Grondelle, R. (1997) Primary electron transfer kinetics in membrane-bound *Rhodobacter* sphaeroides reaction centers: A global and target analysis, *Biochemistry 36*, 11360-11368.
- [63] Pawlowicz, N. P., van Grondelle, R., van Stokkum, I. H. M., Breton, J., Jones, M. R., and Groot, M. L. (2008) Identification of the first steps in charge separation in bacterial photosynthetic reaction centers of *Rhodobacter sphaeroides* by ultrafast mid-infrared spectroscopy: Electron transfer and protein dynamics, *Biophys J* 95, 1268-1284.
- [64] Shkuropatov, A. Y., and Shuvalov, V. A. (1993) Electron transfer in pheophytin *a*-modified reaction centers from *Rhodobacter sphaeroides* (R-26), *FEBS Letters 322*, 168-172.
- [65] Heller, B. A., Holten, D., and Kirmaier, C. (1996) Effects of Asp residues near the L-side pigments in bacterial reaction centers, *Biochemistry 35*, 15418-15427.
- [66] Kennis, J. T. M., Shkuropatov, A. Y., van Stokkum, I. H. M., Gast, P., Hoff, A. J., Shuvalov, V. A., and Aartsma, T. J. (1997) Formation of a long-lived P<sup>+</sup>B<sub>A</sub><sup>-</sup> state in plant pheophytin-exchanged reaction centers of *Rhodobacter sphaeroides* R26 at low temperature, *Biochemistry 36*, 16231–16238.
- [67] Roberts, J. A., Holten, D., and Kirmaier, C. (2001) Primary events in photosynthetic reaction centers with multiple mutations near the photoactive electron carriers, *J Phys Chem B* 105, 5575-5584.
- [68] Kirmaier, C., Laporte, L., Schenck, C. C., and Holten, D. (1995) The nature and dynamics of the charge-separated intermediate in reaction centers in which bacteriochlorophyll replaces the photoactive bacteriopheophytin. 1. Spectral characterization of the transient state, *J Phys Chem* 99, 8903-8909.
- [69] Kirmaier, C., Laporte, L., Schenck, C. C., and Holten, D. (1995) The nature and dynamics of the charge-separated intermediate in reaction centers in which bacteriochlorophyll

- replaces the photoactive bacteriopheophytin. 2. The rates and yields of charge separation and recombination, *J Phys Chem 99*, 8910-8917.
- [70] Deligiannakis, Y., and Rutherford, A. W. (1997) One- and two-dimensional electron spin echo envelope modulation study of the intermediate electron acceptor pheophytin in <sup>14</sup>N-and <sup>15</sup>N-labeled photosystem II, *J Am Chem Soc 119*, 4471–4480.
- [71] Lendzian, F., Mobius, K., and Lubitz, W. (1982) The pheophytin *a* anion radical. <sup>14</sup>N and <sup>1</sup>H ENDOR and triple resonance in liquid solution, *Chem Phys Lett 90*, 375–381.
- [72] Groot, M. L., Pawlowicz, N. P., van Wilderen, L. J. G. W., Breton, J., van Stokkum, I. H. M., and van Grondelle, R. (2005) Initial electron donor and acceptor in isolated photosystem II reaction centers identified with femtosecond mid-IR spectroscopy, *Proc Natl Acad Sci USA 102*, 13087–13092.
- [73] Holzwarth, A. R., Müller, M. G., Reus, M., Nowaczyk, M., Sander, J., and Rögner, M. (2006) Kinetics and mechanism of electron transfer in intact photosystem II and in the isolated reaction center: Pheophytin is the primary electron acceptor, *Proc Natl Acad Sci USA 103*, 6895–6900.
- [74] Shuvalov, V. A., Klevanik, A. V., Sharkov, A. V., Kryukov, P. G., and Bacon, K. E. (1979) Picosecond spectroscopy of photosystem I reaction centers, *FEBS Lett* 107, 313–316.
- [75] Shuvalov, V. A., K.E, B., and Dolan, E. (1979) Kinetic and spectral properties of the intermediary electron acceptor A<sub>1</sub> in photosystem I: Subnanosecond spectroscopy, *FEBS Lett 100*, 5–8.
- [76] Shuvalov, V. A., Dolan, E., and Ke, B. (1979) Spectral and kinetic evidence for two early electron acceptors in photosystem I, *Proc Natl Acad Sci USA* 76, 770–773.
- [77] Ke, B., Shuvalov, V. A., and Dolan, E. (1980) Early reactions in green-plant photosystem I, *Sov J Quantum Electron 10*, 266-270.
- [78] Fenton, J. M., Pellin, M. J., Govindjee, and Kaufmann, K. J. (1979) Primary photochemistry of the reaction center of photosystem I, *FEBS Lett 100*, 1–4.
- [79] Baltimore, B. G., and Malkin, R. (1980) Spectral characterization of the intermediate electron acceptor (A<sub>1</sub>) of photosystem I, *FEBS Lett 110*, 50–52.
- [80] Fong, F. K., Koester, V. J., and Polles, J. S. (1976) Optical spectroscopic study of (Chl  $a\cdot H_2O$ )<sub>2</sub> according to the proposed C<sub>2</sub> symmetrical molecular structure for the P<sub>700</sub> photoactive aggregate in photosynthesis, *J Am Chem Soc* 98, 6406–6408.

- [81] Ikegami, I., Itoh, S., and Iwaki, M. (1995) Photoactive photosystem I particles with a molar ratio of chlorophyll *a* to P<sub>700</sub> of 9, *Plant Cell Physiol 36*, 857–864.
- [82] Heathcote, P., Timofeev, K. N., and Evans, M. C. (1979) Detection by EPR spectrometry of a new intermediate in the primary photochemistry of photosystem I particles isolated using Triton X-100, *FEBS Lett 101*, 105–109.
- [83] Commoner, B., Heise, J. J., and Townsend, J. (1956) Light-induced paramagnetism in chloroplasts *Proc Natl Acad Sci USA 42*, 710–718.
- [84] Norris, J. R., Uphaus, R. A., Crespi, H. L., and Katz, J. J. (1971) Electron spin resonance of chlorophyll and the origin of signal I in photosynthesis, *Proc Natl Acad Sci USA 68*, 625–628.
- [85] Fajer, J., Brune, D. C., Davis, M. S., Forman, A., and Spaulding, L. D. (1975) Primary charge separation in bacterial photosynthesis: oxidized chlorophylls and reduced pheophytin, *Proc Natl Acad Sci USA* 72, 4956–4960.
- [86] Fajer, J., Davis, M. S., Forman, A., Klimov, V. V., Dolan, E., and Ke, B. (1980) Primary electron acceptors in plant photosynthesis, *J Am Chem Soc* 102, 7143–7145.
- [87] Yang, F., Shen, G., Schluchter, W. M., Zybailov, B. L., Ganago, A. O., Vassiliev, I. R., Bryant, D. A., and Golbeck, J. H. (1998) Deletion of the psaF polypeptide modifies the environment of the redox-active phylloquinone (A<sub>1</sub>). Evidence for unidirectionality of electron transfer in photosystem I, *J Phys Chem B* 102, 8288–8299.
- [88] Gorka, M., Charles, P., Kalendra, V., Baldansuren, A., Lakshmi, K. V., and Golbeck, J. H. (2021) A dimeric chlorophyll electron acceptor differentiates type I from type II photosynthetic reaction centers, *iScience 24*, 102719.
- [89] Gorka, M., Gruszecki, E., Charles, P., Kalendra, V., Lakshmi, K. V., and Golbeck, J. H. (2021) Two-dimensional HYSCORE spectroscopy reveals a histidine imidazole as the axial ligand to Chl<sub>3A</sub> in the M688H<sub>PsaA</sub> genetic variant of Photosystem I, *Biochim Biophys Acta Bioenerg* 1862, 148424.
- [90] Johnson, T. W., Zybailov, B., Jones, A. D., Bittl, R., Zech, S., Stehlik, D., Golbeck, J. H., and Chitnis, P. R. (2001) Recruitment of a foreign quinone into the A<sub>1</sub> site of photosystem I, *J Biol Chem* 276, 39512–39521.
- [91] Johnson, T. W., Shen, G., Zybailov, B., Kolling, D., Reategui, R., Beauparlant, S., Vassiliev, I. R., Bryant, D. A., Jones, A. D., Golbeck, J. H., and Chitnis, P. R. (2000)

- Recruitment of a foreign quinone into the A<sub>1</sub> site of photosystem I. I. genetic and physiological characterization of phylloquinone biosynthetic pathway mutants in *Synechocystis* sp. pcc 6803, *J Biol Chem 275*, 8523–8530.
- [92] Johnson, T. W., Zybailov, B., Jones, A. D., Bittl, R., Zech, S., Stehlik, D., Golbeck, J. H., and Chitnis, P. R. (2001) Recruitment of a foreign quinone into the A<sub>1</sub> site of photosystem I. *In vivo* replacement of plastoquinone-9 by media-supplemented naphthoquinones in phylloquinone biosynthetic pathway mutants of *Synechocystis* sp. PCC 6803, *J Biol Chem* 276, 39512–39521.
- [93] Semenov, A. Y., Vassiliev, I. R., van Der Est, A., Mamedov, M. D., Zybailov, B., Shen, G., Stehlik, D., Diner, B. A., Chitnis, P. R., and Golbeck, J. H. (2000) Recruitment of a foreign quinone into the A<sub>1</sub> site of photosystem I. Altered kinetics of electron transfer in phylloquinone biosynthetic pathway mutants studied by time-resolved optical, EPR, and electrometric techniques, *J Biol Chem* 275, 23429–23438.
- [94] Itoh, S., Iwaki, M., and Ikegami, I. (1987) Extraction of vitamin K-1 from photosystem I particles by treatment with diethyl ether and its effects on the A<sub>-1</sub> EPR signal and system I photochemistry, *Biochim Biophys Acta Bioenerg* 893, 508–516.
- [95] Ikegami, I., Sétif, P., and Mathis, P. (1987) Absorption studies of photosystem I photochemistry in the absence of vitamin K-1, *Biochim Biophys Acta, Bioenerg 894*, 414–422.
- [96] Sun, J., Hao, S., Radle, M., Xu, W., Shelaev, I., Nadtochenko, V., Shuvalov, V., Semenov, A., Gordon, H., van der Est, A., and Golbeck, J. H. (2014) Evidence that histidine forms a coordination bond to the A<sub>0A</sub> and A<sub>0B</sub> chlorophylls and a second H-bond to the A<sub>1A</sub> and A<sub>1B</sub> phylloquinones in M688H<sub>PsaA</sub> and M668H<sub>PsaB</sub> variants of *Synechocystis* sp. PCC 6803, *Biochim Biophys Acta Bioenerg 1837*, 1362–1375.
- [97] Guergova-Kuras, M., Boudreaux, B., Joliot, A., Joliot, P., and Redding, K. (2001) Evidence for two active branches for electron transfer in photosystem I, *Proc Natl Acad Sci U S A 98*, 4437–4442.
- [98] Shelaev, I. V., Gostev, F. E., Mamedov, M. D., Sarkisov, O. M., Nadtochenko, V. A., Shuvalov, V. A., and Semenov, A. Y. (2010) Femtosecond primary charge separation in *Synechocystis* sp. PCC 6803 photosystem I, *Biochim Biophys Acta 1797*, 1410–1420.

- [99] Fajer, J., Fujita, I., Davis, M. S., Forman, A., Hanson, L. K., Smith, K. M., and M., K. K. (1982) Electrochemical and spectrochemical studies of biological redox components In *ACS division of analytical chemistry* (Km, K., Ed.), pp 489–513, Atlanta, GA.
- [100] Orf, G. S., Gisriel, C., and Redding, K. E. (2018) Evolution of photosynthetic reaction centers: Insights from the structure of the heliobacterial reaction center, *Photosynth Res* 138, 11–37.
- [101] Ferlez, B., Cowgill, J., Dong, W., Gisriel, C., Lin, S., Flores, M., Walters, K., Cetnar, D., Redding, K. E., and Golbeck, J. H. (2016) Thermodynamics of the electron acceptors in *Heliobacterium modesticaldum*: An exemplar of an early homodimeric Type I photosynthetic reaction center, *Biochemistry* 55, 2358–2370.
- [102] Taylor, N., and Kassal, I. (2019) Why are photosynthetic reaction centres dimeric?, *Chem Sci* 10, 9576–9585.
- [103] Kobayashi, M., Ohashi, S., Iwamoto, K., Shiraiwa, Y., Kato, Y., and Watanabe, T. (2007) Redox potential of chlorophyll *d in vitro*, *Biochim Biophys Acta, Bioenerg* 1767, 596–602.
- [104] Deisenhofer, J., Epp, O., Sinning, I., and Michel, H. (1995) Crystallographic refinement at 2.3 Å resolution and refined model of the photosynthetic reaction centre from *Rhodopseudomonas viridis*, J Mol Biol 246, 429–457.
- [105] Bowes, J., Crofts, A. R., and Arntzen, C. J. (1980) Redox reactions on the reducing side of photosystem II in chloroplasts with altered herbicide binding properties, *Arch Biochem Biophys* 200, 303–308.
- [106] Robinson, H. H., and Crofts, A. R. (1983) Kinetics of the oxidation—reduction reactions of the photosystem II quinone acceptor complex, and the pathway for deactivation, *FEBS Letters* 153, 221-226.
- [107] Gopta, O. A., Cherepanov, D. A., Mulkidjanian, A. Y., Semenov, A. Y., and Bloch, D. A. (1998) Effect of temperature and surface potential on the electrogenic proton uptake in the  $Q_B$  site of the *Rhodobacter sphaeroides* photosynthetic reaction center:  $Q_A^{-\bullet B^{-\bullet}} \rightarrow Q_A Q_B H_2$  transition, *Photosyn Res* 55, 309–316.
- [108] Mulkidjanian, A. Y., Kozlova, M. A., and Cherepanov, D. A. (2005) Ubiquinone reduction in the photosynthetic reaction centre of *Rhodobacter sphaeroides:* interplay between electron transfer, proton binding and flips of the quinone ring, *Biochem Soc Trans 33*, 845–850.

- [109] Wei, R. J., Zhang, Y., Mao, J., Kaur, D., Khaniya, U., and Gunner, M. R. (2022) Comparison of proton transfer paths to the Q<sub>A</sub> and Q<sub>B</sub> sites of the *Rba. sphaeroides* photosynthetic reaction centers, *Photosyn Res*.
- [110] Katilius, E., Babendure, J. L., Lin, S., and Woodbury, N. W. (2004) Electron transfer dynamics in *Rhodobacter sphaeroides* reaction center mutants with a modified ligand for the monomer bacteriochlorophyll on the active aide, *Photosyn Res 81*, 165–180.
- [111] Vinyard, D. J., Ananyev, G. M., and Charles Dismukes, G. (2013) Photosystem II: The reaction center of oxygenic photosynthesis, *Annu Rev Biochem* 82, 577–606.
- [112] Lakshmi, K. V., Coates, C. S., Smith, S., and Chatterjee, R. (2014) The Radical Intermediates of Photosystem II, In *The Biophysics of Photosynthesis* (Golbeck, J., and van der Est, A., Eds.), pp 299-320, Springer New York, New York, NY.
- [113] Croce, R., and van Amerongen, H. (2017) The complex that conquered the land, *Science* 357, 752.
- [114] Kato, K., Miyazaki, N., Hamaguchi, T., Nakajima, Y., Akita, F., Yonekura, K., and Shen, J.-R. (2021) High-resolution cryo-EM structure of photosystem II reveals damage from high-dose electron beams, *Commun Biol 4*, 382.
- [115] Li, M., Ma, J., Li, X., and Sui, S.-F. (2021) *In situ* cryo-ET structure of phycobilisome—photosystem II supercomplex from red alga, *eLife 10*, e69635.
- [116] Yu, H., Hamaguchi, T., Nakajima, Y., Kato, K., Kawakami, K., Akita, F., Yonekura, K., and Shen, J.-R. (2021) Cryo-EM structure of monomeric photosystem II at 2.78 Å resolution reveals factors important for the formation of dimer, *Biochim Biophys Acta Bioenerg* 1862, 148471.
- [117] Gisriel, C. J., Wang, J., Liu, J., Flesher, D. A., Reiss, K. M., Huang, H.-L., Yang, K. R., Armstrong, W. H., Gunner, M. R., Batista, V. S., Debus, R. J., and Brudvig, G. W. (2022) High-resolution cryo-electron microscopy structure of photosystem II from the mesophilic cyanobacterium, *Synechocystis* sp. PCC 6803, *Proc Natl Acad Sci USA 119*, e2116765118.
- [118] Käβ, H., Bittersmann-Weidlich, E., Andréasson, L. E., Bönigk, B., and Lubitz, W. (1995) ENDOR and ESEEM of the <sup>15</sup>N labelled radical cations of chlorophyll *a* and the primary donor P<sub>700</sub> in photosystem I, *Chem Phys 194*, 419–432.

- [119] Kä $\beta$ , H., Fromme, P., and Lubitz, W. (1996) Quadrupole parameters of nitrogen nuclei in the cation radical  $P_{700}$ . determined by ESEEM of single crystals of photosystem I, *Chem Phys Lett* 257, 197–206.
- [120] Käβ, H., and Lubitz, W. (1996) Evaluation of 2D ESEEM data of <sup>15</sup>N-labeled radical cations of the primary donor P<sub>700</sub> in photosystem I and chlorophyll *a*, *Chem Phys Lett 251*, 193–203.
- [121] Dorlet, P., Xiong, L., Sayre, R. T., and Un, S. (2001) High field EPR study of the pheophytin anion radical in wild type and D1-E130 mutants of photosystem II in *Chlamydomonas reinhardtii J Biol Chem* 276, 22313–22316.
- [122] Rutherford, A. W. (1981) EPR evidence for an acceptor functioning in photosystem II when the pheophytin acceptor is reduced, *Biochem Biophys Res Commun* 102, 1065–1070.
- [123] Klimov, V. V., Dolan, E., Shaw, E. R., and Ke, B. (1980) Interaction between the intermediary electron acceptor (pheophytin) and a possible plastoquinone-iron complex in photosystem II reaction centers, *Proc Natl Acad Sci USA* 77, 7227–7231.
- [124] Forman, A., Davis, M. S., Fujita, I., Hanson, L. K., Smith, K. M., and Fajer, J. (1981) Mechanisms of energy transduction in plant photosynthesis: ESR, ENDOR and MOs of the primary acceptors, *Isr J Chem 21*, 265–269.
- [125] Mansfield, R. W., and Evans, M. C. W. (1985) Optical difference spectrum of the electron acceptor A<sub>0</sub> in photosystem I, *FEBS Lett 190*, 237–241.
- [126] Ikegami, I., and Ke, B. (1984) A 160-kilodalton photosystem-I reaction-center complex. Low-temperature absorption and EPR spectroscopy of the early electron acceptors, *Biochim Biophys Acta Bioenerg* 764, 70–79.
- [127] Norris, J. R., Scheer, H., Druyan, M. E., and Katz, J. J. (1974) An electron-nuclear double resonance (ENDOR) study of the special pair model for photo-reactive chlorophyll in photosynthesis, *Proc Natl Acad Sci USA 71*, 4897–4900.
- [128] Lin, C. P., Bowman, M. K., and Norris, J. R. (1986) Analysis of electron spin echo modulation in randomly oriented solids: <sup>15</sup>N modulation of radical cations of bacteriochlorophyll *a* and the primary donor of photosynthetic bacterium *Rhodospirillum rubrum*, *J Chem Phys* 85, 56–62.

- [129] Hofbauer, W., Zouni, A., Bittl, R., Kern, J., Orth, P., Lendzian, F., Fromme, P., Witt, H. T., and Lubitz, W. (2001) Photosystem II single crystals studied by EPR spectroscopy at 94 GHz: The tyrosine radical Y<sub>D</sub>, *Proc Natl Acad Sci USA 98*, 6623–6628.
- [130] Britt, R. D., Campbell, K. A., Peloquin, J. M., Gilchrist, M. L., Aznar, C. P., Dicus, M. M., Robblee, J., and Messinger, J. (2004) Recent pulsed EPR studies of the photosystem II oxygen-evolving complex: implications as to water oxidation mechanisms, *Biochim Biophys Acta Bioenerg* 1655, 158–171.
- [131] Stich, T. A., Yeagle, G. J., Service, R. J., Debus, R. J., and Britt, R. D. (2011) Ligation of D1-His332 and D1-Asp170 to the manganese cluster of photosystem II from *Synechocystis* assessed by multifrequency pulse EPR spectroscopy, *Biochemistry* 50, 7390–7404.
- [132] Tang, J., Utschig, L. M., Poluektov, O., and Thurnauer, M. C. (1999) Transient W-band EPR study of sequential electron transfer in photosynthetic bacterial reaction centers, *J Phys Chem B* 103, 5145–5150.
- [133] Utschig, L. M., Greenfield, S. R., Tang, J., Laible, P. D., and Thurnauer, M. C. (1997) Influence of iron-removal procedures on sequential electron transfer in photosynthetic bacterial reaction centers Studied by transient EPR spectroscopy, *Biochemistry* 36, 8548–8558.
- [134] Chatterjee, R., Milikisiyants, S., Coates, C. S., and Lakshmi, K. V. (2011) High-resolution two-dimensional <sup>1</sup>H and <sup>14</sup>N hyperfine sublevel correlation spectroscopy of the primary quinone of photosystem II, *Biochemistry* 50, 491–501.
- [135] Davis, I. H., Heathcote, P., MacLachlan, D. J., and Evans, M. C. W. (1993) Modulation analysis of the electron spin echo signals of *in vivo* oxidised primary donor <sup>14</sup>N chlorophyll centres in bacterial, P<sub>870</sub> and P<sub>960</sub>, and plant photosystem I, P<sub>700</sub>, reaction centres, *Biochim Biophys Acta Bioenerg 1143*, 183–189.
- [136] Mac, M., Bowlby, N. R., Babcock, G. T., and McCracken, J. (1998) Monomeric spin density distribution in the primary donor of photosystem I as determined by electron magnetic resonance: Functional and thermodynamic implications, *J Am Chem Soc 120*, 13215–13223.
- [137] Käss, H., Fromme, P., Witt, H. T., and Lubitz, W. (2001) Orientation and electronic structure of the primary donor radical cation in photosystem I: A single crystals EPR and ENDOR Study, *J Phys Chem B* 105, 1225–1239.

- [138] van Gorkom, H. J., Tamminga, J. J., and Haveman, J. (1974) Primary reactions, plastoquinone and fluorescence yield in subchloroplast fragments prepared with deoxycholate, *Biochim Biophys Acta 347*, 417–438.
- [139] Davis, M. S., Forman, A., and Fajer, J. (1979) Ligated chlorophyll cation radicals: Their function in photosystem II of plant photosynthesis, *Proc Natl Acad Sci USA 76*, 4170–4174.
- [140] Harmer, J., Mitrikas, G., and Schweiger, A. (2009) Advanced pulse EPR methods for the characterization of metalloproteins, In *High Resolution EPR: Applications to Metalloenzymes and Metals in Medicine* (Berliner, L., and Hanson, G., Eds.), pp 13–61, Springer New York, New York, NY.
- [141] Prisner, T., Rohrer, M., and MacMillan, F. (2001) Pulsed EPR spectroscopy: Biological applications, *Annu Rev Phys Chem 52*, 279–313.
- [142] Deligiannakis, Y., Louloudi, M., and Hadjiliadis, N. (2000) Electron spin echo envelope modulation (ESEEM) spectroscopy as a tool to investigate the coordination environment of metal centers, *J Coord Chem 204*, 1–112.
- [143] Lakshmi, K. V., and Brudvig, G. W. (2001) Pulsed electron paramagnetic resonance methods for macromolecular structure determination, *Curr Opin Struct Biol* 11, 523–531.
- [144] Lakshmi, K. V., and Brudvig, G. W. (2000) Electron paramagnetic resonance distance measurements in photosystems, In *Distance Measurements in Biological Systems by EPR* (Berliner, L. J., Eaton, G. R., and Eaton, S. S., Eds.), pp 513–567, Springer US, Boston, MA.
- [145] Britt, R. D. (1993) Time-domain electron paramagnetic resonance spectroscopy, *Curr Opin Struct Biol* 3, 774–779.
- [146] Milikisiyants, S., Chatterjee, R., Weyers, A., Meenaghan, A., Coates, C., and Lakshmi, K. V. (2010) Ligand environment of the S2 state of photosystem II: a study of the hyperfine interactions of the tetranuclear manganese cluster by 2D <sup>14</sup>N HYSCORE spectroscopy, *J Phys Chem B* 114, 10905–10911.
- [147] Milikisiyants, S., Chatterjee, R., Coates, C. S., Koua, F. H. M., Shen, J.-R., and Lakshmi, K. V. (2012) The structure and activation of substrate water molecules in the S<sub>2</sub> state of photosystem II studied by hyperfine sublevel correlation spectroscopy, *Energy Environ Sci* 5, 7747–7756.

- [148] Chatterjee, R., Coates, C. S., Milikisiyants, S., Lee, C. I., Wagner, A., Poluektov, O. G., and Lakshmi, K. V. (2013) High-frequency electron nuclear double-resonance spectroscopy studies of the mechanism of proton-coupled electron transfer at the tyrosine-D residue of photosystem II, *Biochemistry* 52, 4781–4790.
- [149] Taguchi, A. T., O'Malley, P. J., Wraight, C. A., and Dikanov, S. A. (2014) Nuclear hyperfine and quadrupole tensor characterization of the nitrogen hydrogen bond donors to the semiquinone of the Q<sub>B</sub> site in bacterial reaction centers: a combined X- and S-band (14,15)N ESEEM and DFT study, *J Phys Chem B 118*, 1501–1509.
- [150] Borovykh, I. V., Dzuba, S. A., Proskuryakov, I. I., Gast, P., and Hoff, A. J. (1998) Light-induced structural changes in photosynthetic reaction centres studied by ESEEM of spin-correlated D<sup>+</sup>Q<sub>A</sub><sup>-</sup> radical pairs, *Biochim Biophys Acta Bioenerg* 1363, 182–186.
- [151] Deligiannakis, Y., and Rutherford, A. W. (2001) Electron spin echo envelope modulation spectroscopy in photosystem I, *Biochim Biophys Acta Bioenerg* 1507, 226–246.
- [152] Coates, C. S., Milikisiyants, S., Chatterjee, R., Whittaker, M. M., Whittaker, J. W., and Lakshmi, K. V. (2015) Two-dimensional HYSCORE spectroscopy of superoxidized manganese catalase: a model for the oxygen-evolving complex of photosystem II, *J Phys Chem B* 119, 4905–4916.
- [153] Chestnut, M. M., Milikisiyants, S., Chatterjee, R., Kern, J., and Smirnov, A. I. (2021) Electronic structure of the primary electron donor  $P_{700}^{+\bullet}$  in photosystem I studied by multifrequency HYSCORE spectroscopy at X- and Q-Band, *J Phys Chem B* 125, 36–48.
- [154] Chrysina, M., Zahariou, G., Ioannidis, N., Sanakis, Y., and Mitrikas, G. (2021) Electronic structure of tyrosyl D radical of photosystem II, as revealed by 2D-hyperfine sublevel correlation spectroscopy, *Magnetochemistry* 7, 131.
- [155] Webber, A. N., and Lubitz, W. (2001) P<sub>700</sub>: the primary electron donor of photosystem I, *Biochim Biophys Acta Bioenerg* 1507, 61–79.
- [156] Mims, W. B. (1965) Pulsed ENDOR experiments, *Proc R Soc Lond Series A. Math Phys Sci* 283, 452–457.
- [157] Höfer, P., Grupp, A., Nebenführ, H., and Mehring, M. (1986) Hyperfine sublevel correlation (HYSCORE) spectroscopy: a 2D ESR investigation of the squaric acid radical, *Chem Phys Lett* 132, 279–282.

- [158] Kok, B. (1956) On the reversible absorption change at 705 mu in photosynthetic organisms, *Biochim Biophys Acta* 22, 399–401.
- [159] Fromme, P., and Mathis, P. (2004) Unraveling the photosystem I reaction center: A history, or the sum of many efforts, *Photosyn Res* 80, 109–124.
- [160] Pérez, A. A., Ferlez, B. H., Applegate, A. M., Walters, K., He, Z., Shen, G., Golbeck, J. H., and Bryant, D. A. (2018) Presence of a [3Fe–4S] cluster in a PsaC variant as a functional component of the photosystem I electron transfer chain in *Synechococcus* sp. PCC 7002, *Photosyn Res* 136, 31–48.
- [161] Berthold, T., Donner von Gromoff, E., Santabarbara, S., Stehle, P., Link, G., Poluektov, O. G., Heathcote, P., Beck, C. F., Thurnauer, M. C., and Kothe, G. (2012) Exploring the electron transfer pathways in photosystem I by high-time-resolution electron paramagnetic resonance: observation of the B-side radical pair  $P_{700}^{+}A_{1B}^{-}$  in whole cells of the deuterated green alga *Chlamydomonas reinhardtii* at cryogenic temperatures, *J Am Chem Soc 134*, 5563–5576.
- [162] Srinivasan, N., Santabarbara, S., Rappaport, F., Carbonera, D., Redding, K., van der Est, A., and Golbeck, J. H. (2011) Alteration of the H-bond to the A<sub>1A</sub> phylloquinone in photosystem I: Influence on the kinetics and energetics of electron transfer, *J Phys Chem B* 115, 1751–1759.
- [163] Srinivasan, N., Karyagina, I., Bittl, R., van der Est, A., and Golbeck, J. H. (2009) Role of the hydrogen bond from Leu722 to the A<sub>1A</sub> phylloquinone in photosystem I, *Biochemistry* 48, 3315–3324.
- [164] van der Est, A., Chirico, S., Karyagina, I., Cohen, R., Shen, G., and Golbeck, J. H. (2009) Alteration of the axial Met ligand to electron acceptor A<sub>0</sub> in photosystem I: An investigation of electron transfer at different temperatures by multifrequency time-resolved and CW EPR, *Appl Magn Reson 37*, 103.
- [165] Chirico, S., Drago, E., Golbeck, J. H., Johnson, W., and van der Est, A., (Eds.) (2008) Transient EPR studies of in vivo uptake of substituted anthraquinones by photosystem I in phylloquinone biosynthetic pathway mutants of Synechocystis sp. PCC 6803, Springer Netherlands, Dordrecht.

- [166] Karyagina, I., Golbeck, J. H., Srinivasan, N., Stehlik, D., and Zimmermann, H. (2006) Single-sided hydroge bonding to the quinone cofactor in photosystem I probed by selective <sup>13</sup>C-labelled naphthoquinones and transient EPR, *Appl Magn Reson 30*, 287–310.
- [167] Pushkar, Y. N., Ayzatulin, O., and Stehlik, D. (2005) Transient and pulsed EPR study of <sup>17</sup>O-substituted methyl-naphthoquinone as radical anion in the A<sub>1</sub> binding site of photosystem I and in frozen solution, *Appl Magn Reson 28*, 195–211.
- [168] Petrenko, A., Maniero, A. L., van Tol, J., MacMillan, F., Li, Y., Brunel, L.-C., and Redding, K. (2004) A high-field EPR study of P<sub>700</sub><sup>+•</sup> in wild-type and mutant photosystem I from *Chlamydomonas reinhardtii*, *Biochemistry 43*, 1781–1786.
- [169] Ferlez, B., Agostini, A., Carbonera, D., Golbeck, J. H., and van der Est, A. (2017) Triplet charge recombination in heliobacterial reaction centers does not produce a spin-polarized EPR spectrum, *Z Phys Chem 231*, 593–607.
- [170] Ferlez, B., Dong, W., Siavashi, R., Redding, K., Hou, H. J. M., Golbeck, J. H., and van der Est, A. (2015) The effect of bacteriochlorophyll *g* oxidation on energy and electron transfer in reaction centers from *Heliobacterium modesticaldum*, *J Phys Chem B* 119, 13714–13725.
- [171] Nitschke, W., Feiler, U., and Rutherford, A. W. (1990) Photosynthetic reaction center of green sulfur bacteria studied by EPR, *Biochemistry* 29, 3834–3842.
- [172] Hager-Braun, C., Jarosch, U., Hauska, G., Nitschke, W., and Riedel, A. (1997) EPR studies of the terminal electron acceptors of the green sulfur bacterial reaction centre. Revisited, *Photosyn Res* 51, 127–136.
- [173] van der Est, A., Hager-Braun, C., Leibl, W., Hauska, G., and Stehlik, D. (1998) Transient electron paramagnetic resonance spectroscopy on green-sulfur bacteria and heliobacteria at two microwave frequencies, *Biochim Biophys Acta Bioenerg* 1409, 87–98.
- [174] García-Rubio, I., Martínez, J. I., Picorel, R., Yruela, I., and Alonso, P. J. (2003) HYSCORE spectroscopy in the cytochrome b<sub>559</sub> of the photosystem II reaction center, *J Am Chem Soc* 125, 15846–15854.
- [175] van Doorslaer, S. (2017) Understanding heme proteins with hyperfine spectroscopy, *J Magn Reson 280*, 79–88.

- [176] Hoff, A. J., Lendzian, F., Möbius, K., and Lubitz, W. (1982) Proton and nitrogen electron nuclear double and triple resonance of the chlorophyll a anion in liquid solution, *Chem Phys Lett* 85, 3–8.
- [177] Dunham, W. R., Bearden, A. J., Salmeen, I. T., Palmer, G., Sands, R. H., Orme-Johnson, W. H., and Beinert, H. (1971) The two-iron ferredoxins in spinach, parsley, pig adrenal cortex, *Azotobacter vinelandii*, and *Clostridium pasteurianum*: studies by magnetic field Mössbauer spectroscopy, *Biochim Biophys Acta Bioenerg* 253, 134–152.
- [178] Becke, A. D. (1988) Density-functional exchange-energy approximation with correct asymptotic behavior, *Phys Rev A* 38, 3098–3100.
- [179] Lee, C., Yang, W., and Parr, R. G. (1988) Development of the Colle-Salvetti correlationenergy formula into a functional of the electron density, *Phys Rev B* 37, 785–789.
- [180] Barone, V. (1995) Structure, magnetic properties and reactivities of open-shell species from density functional and self-consistent hybrid methods, In *Recent Advances in Density Functional Methods*, pp 287–334.
- [181] Weigend, F., and Ahlrichs, R. (2005) Balanced basis sets of split valence, triple zeta valence and quadruple zeta valence quality for H to Rn: design and assessment of accuracy, *Phys Chem Chem Phys* 7, 3297–3305.
- [182] Schäfer, A., Horn, H., and Ahlrichs, R. (1992) Fully optimized contracted Gaussian basis sets for atoms Li to Kr, *J Chem Phys* 97, 2571–2577.
- [183] Weigend, F. (2006) Accurate Coulomb-fitting basis sets for H to Rn, *Phys Chem Chem Phys* 8, 1057–1065.
- [184] Staroverov, V. N., Scuseria, G. E., Tao, J., and Perdew, J. P. (2003) Comparative assessment of a new nonempirical density functional: Molecules and hydrogen-bonded complexes, *J Chem Phys* 119, 12129–12137.
- [185] Neese, F., Wennmohs, F., Hansen, A., and Becker, U. (2009) Efficient, approximate and parallel Hartree–Fock and hybrid DFT calculations. A 'chain-of-spheres' algorithm for the Hartree–Fock exchange, *Chem Phys* 356, 98–109.
- [186] Klamt, A., and Schüürmann, G. (1993) COSMO: A new approach to dielectric screening in solvents with explicit expressions for the screening energy and its gradient, *J Chem Soc Perkin Trans* 2, 799–805.

- [187] Cossi, M., Rega, N., Scalmani, G., and Barone, V. (2003) Energies, structures, and electronic properties of molecules in solution with the C-PCM solvation model, *J Comput Chem* 24, 669–681.
- [188] Sirohiwal, A., Neese, F., and Pantazis, D. A. (2020) Protein matrix control of reaction center excitation in photosystem II, *J Am Chem Soc* 142, 18174–18190.
- [189] Sinnecker, S., Koch, W., and Lubitz, W. (2002) Chlorophyll a radical ions: A density functional study, *J Phys Chem B* 106, 5281–5288.
- [190] Plato, M., Krauß, N., Fromme, P., and Lubitz, W. (2003) Molecular orbital study of the primary electron donor P<sub>700</sub> of photosystem I based on a recent X-ray single crystal structure analysis, *Chem Phys* 294, 483–499.
- [191] Parusel, A. B. J., and Grimme, S. (2000) A theoretical study of the excited states of chlorophyll a and pheophytin a, *J Phys Chem B* 104, 5395–5398.
- [192] O'Malley, P. J. (2000) The effect of oxidation and reduction of chlorophyll *a* on its geometry, vibrational and spin density properties as revealed by hybrid density functional methods, *J Am Chem Soc* 122, 7798–7801.
- [193] Huber, M. (2001) The role of the electronic structure of the porphyrin as viewed by EPR/ENDOR methods in the efficiency of biomimetic model compounds for photosynthesis, *Eur J Org Chem 2001*, 4379–4389.
- [194] Sinnecker, S., Koch, W., and Lubitz, W. (2000) Bacteriochlorophyll a radical cation and anion—calculation of isotropic hyperfine coupling constants by density functional methods, *Phys Chem Chem Phys* 2, 4772–4778.
- [195] O'Malley, P. J., and Collins, S. J. (2001) The effect of axial Mg ligation on the geometry and spin density distribution of chlorophyll and bacteriochlorophyll cation free radical models: A density functional study, *J Am Chem Soc* 123, 11042–11046.
- [196] Orf, G. S., and Redding, K. E. (2021) Perturbation of the primary acceptor chlorophyll site in the heliobacterial reaction center by coordinating amino acid substitution, *Biochim Biophys Acta Bioenerg* 1862, 148324.
- [197] Ermler, U., Fritzsch, G., Buchanan, S. K., and Michel, H. (1994) Structure of the photosynthetic reaction centre from *Rhodobacter sphaeroides* at 2.65 Å resolution: Cofactors and protein-cofactor interactions, *Structure* 2, 925–936.

- [198] Lubitz, W., Isaacson, R. A., Okamura, M. Y., Abresch, E. C., Plato, M., and Feher, G. (1989) ENDOR studies of the intermediate electron acceptor radical anion I in photosystem II reaction centers, *Biochim Biophys Acta Bioenerg* 977, 227–232.
- [199] O'Malley, P. J. (2000) Hybrid density functional studies of pheophytin anion radicals: Implications for initial electron transfer in photosynthetic reaction centers, *J Phys Chem B* 104, 2176–2182.
- [200] O'Malley, P. J. (1999) The electronic structure of the bacteriopheophytin *a* anion radical, *in vivo*, *J Am Chem Soc 121*, 3185–3192.
- [201] Geskes, C., Meyer, M., Fischer, M., Scheer, H., and Heinze, J. (1995) Electrochemical investigation of modified photosynthetic pigments, *J Phys Chem B* 99, 17669–17672.
- [202] Huber, H., Meyer, M., Nägele, T., Hartl, I., Scheer, H., Zinth, W., and Wachtveitl, J. (1995) Primary photosynthesis in reaction centers containing four different types of electron acceptors at site H<sub>A</sub>, *Chem Phys* 197, 297–305.
- [203] Huber, H., Meyer, M., Scheer, H., Zinth, W., and Wachtveitl, J. (1998) Temperature dependence of the primary electron transfer reaction in pigment-modified bacterial reaction centers, *Photosyn Res* 55, 153–162.
- [204] Wachtveitl, J., Huber, H., Feick, R., Rautter, J., Müh, F., and Lubitz, W. (1998) Electron transfer in bacterial reaction centers with an energetically raised primary acceptor: ultrafast spectroscopy and ENDOR/TRIPLE studies, *Spectrochim Acta A Mol Biomol Spectrosc* 54, 1231–1245.
- [205] de Wijn, R., and van Gorkom, H. J. (2001) Kinetics of electron transfer from Q(a) to Q(b) in photosystem II, *Biochemistry 40*, 11912-11922.
- [206] Cardona, T. (2016) Reconstructing the origin of oxygenic photosynthesis: Do assembly and photoactivation recapitulate evolution?, *Front Plant Sci* 7.
- [207] Rutherford, A. W., Osyczka, A., and Rappaport, F. (2012) Back-reactions, short-circuits, leaks and other energy wasteful reactions in biological electron transfer: Redox tuning to survive life in O<sub>2</sub>, *FEBS Lett 586*, 603–616.
- [208] Cardona, T. (2016) Reconstructing the origin of oxygenic photosynthesis: do assembly and photoactivation recapitulate evolution?, *Front Plant Sci* 7.

- [209] Brütting, M., Foerster, J. M., and Kümmel, S. (2021) Investigating primary charge separation in the reaction center of *Heliobacterium modesticaldum*, *J Phys Chem B 125*, 3468–3475.
- [210] Badshah, S. L., Sun, J., Mula, S., Gorka, M., Baker, P., Luthra, R., Lin, S., van der Est, A., Golbeck, J. H., and Redding, K. E. (2018) Mutations in algal and cyanobacterial photosystem I that independently affect the yield of initial charge separation in the two electron transfer cofactor branches, *Biochim Biophys Acta Bioenerg* 1859, 42-55.
- [211] Schlodder, E., Falkenberg, K., Gergeleit, M., and Brettel, K. (1998) Temperature dependence of forward and reverse electron transfer from A<sub>1</sub><sup>-</sup>, the reduced secondary electron acceptor in photosystem I, *Biochemistry 37*, 9466–9476.
- [212] Milanovsky, G., Gopta, O., Petrova, A., Mamedov, M., Gorka, M., Cherepanov, D., Golbeck, J. H., and Semenov, A. (2019) Multiple pathways of charge recombination revealed by the temperature dependence of electron transfer kinetics in cyanobacterial photosystem I, *Biochim Biophys Acta Bioenerg* 1860, 601–610.
- [213] Gorka, M., Cherepanov, D. A., Semenov, A. Y., and Golbeck, J. H. (2020) Control of electron transfer by protein dynamics in photosynthetic reaction centers, *Crit Rev Biochem Mol Biol* 55, 425–468.
- [214] Malferrari, M., Savitsky, A., Lubitz, W., Mobius, K., and Venturoli, G. (2016) Protein immobilization capabilities of sucrose and trehalose glasses: the effect of protein/sugar concentration unraveled by high-field EPR, *J Phys Chem Lett* 7, 4871–4877.